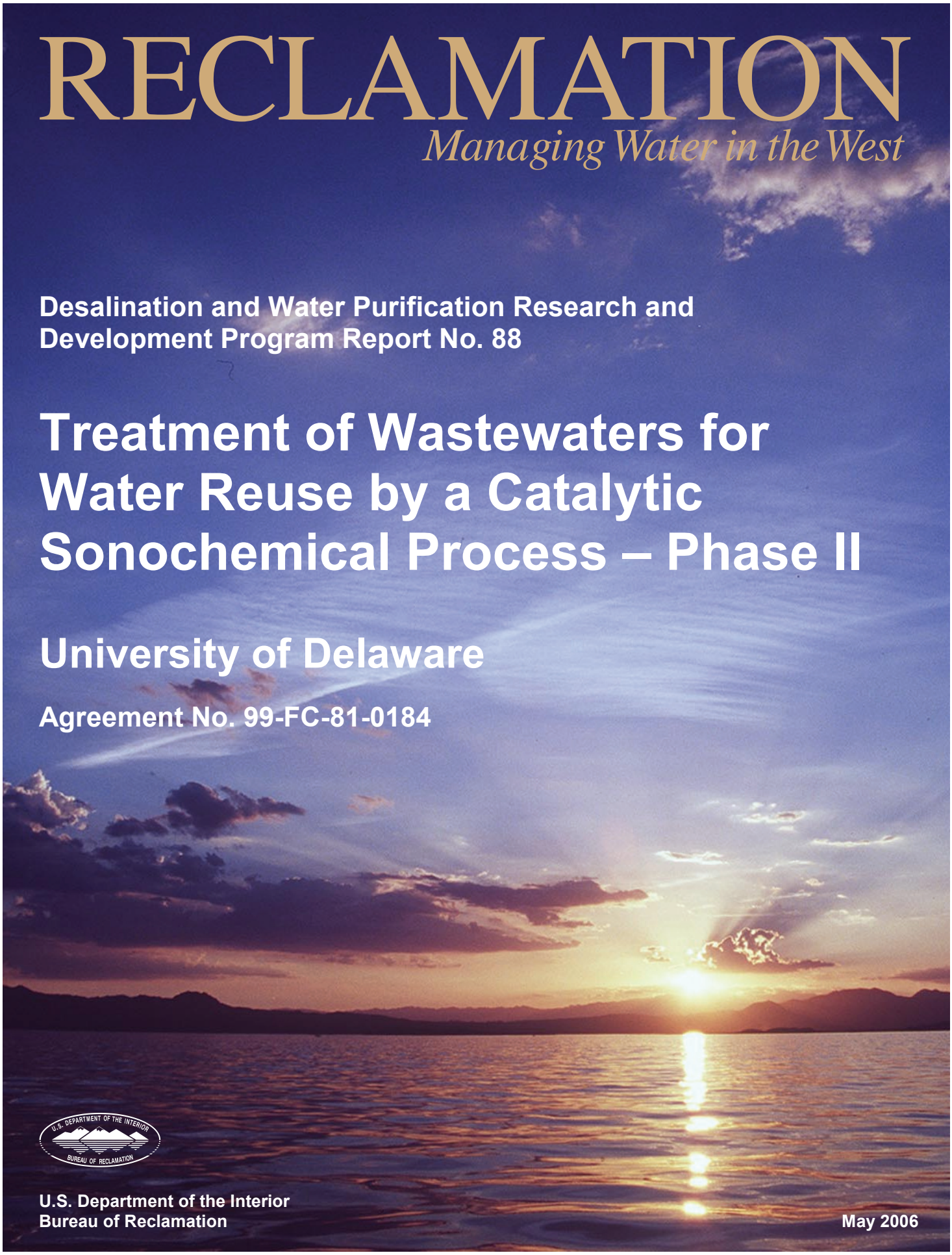

RECLAMATION

Managing Water in the West

Desalination and Water Purification Research and Development Program Report No. 88

Treatment of Wastewaters for Water Reuse by a Catalytic Sonochemical Process – Phase II

University of Delaware

Agreement No. 99-FC-81-0184

U.S. Department of the Interior
Bureau of Reclamation

May 2006

REPORT DOCUMENTATION PAGE

Form Approved
OMB No. 0704-0188

1. REPORT DATE *(DD-MM-YYYY)*	2. REPORT TYPE	3. DATES COVERED *(From - To)*
May 2006	Final	Oct. 15,1999 - Oct. 15, 2001

4. TITLE AND SUBTITLE
Treatment of Wastewaters for Water Reuse by a Catalytic Sonochemical Process – Phase II

5a. CONTRACT NUMBER
99-FC-81-0184

5b. GRANT NUMBER

5c. PROGRAM ELEMENT NUMBER

6. AUTHOR(S)
C.P. Huang (Principal Investigator)
Pei Chiu (Co-Principal Investigator)
Samuel P. Myoda (Graduate Research Assistant)

5d. PROJECT NUMBER

5e. TASK NUMBER

5f. WORK UNIT NUMBER

7. PERFORMING ORGANIZATION NAME(S) AND ADDRESS(ES)
Department of Civil and Environmental Engineering
University of Delaware

8. PERFORMING ORGANIZATION REPORT NUMBER

9. SPONSORING / MONITORING AGENCY NAME(S) AND ADDRESS(ES)
U.S. Department of the Interior, Bureau of Reclamation,
Technical Service Center, Environmental Services Division,
Water Treatment Engineering and Research Group, 86-68230,
PO Box 25007, Denver CO 80228

10. SPONSOR/MONITOR'S ACRONYM(S)

11. SPONSOR/MONITOR'S REPORT NUMBER(S)
Report No. 88

12. DISTRIBUTION / AVAILABILITY STATEMENT
Available from the National Technical Information Service (NTIS),
Operations Division, 5285 Port Royal Road, Springfield VA 22161

13. SUPPLEMENTARY NOTES

14. ABSTRACT ***(Maximum 200 words)***

The second year of the project; Wastewater Reuse by a Catalytic Sonochemical Process was spent designing and refining a pilot plant scale reactor that could efficiently and cost effectively take advantage of the capabilities of the ultrasonic process to disinfect and to oxidize the organic contaminants typically found in waste water effluent. In addition to completing work on the reactor, the modified qualification and quantification methodology based on EPA Method 1623 for *Cryptosporidium parvum* was finalized.

The prototype of the dual filter set was improved to include a second lamp so that simultaneous ultraviolet and visible light excitation is possible. Using this setup, Fluorescein (FITC) labeled oocysts and 4', 6-diamidino-2-phenylindole (DAPI) or Hoechst 33342 stained sporozoites can be viewed at the same time, substantially reducing analysis time and improving accuracy.

A Nearfield™ Acoustical Processor was purchased to scale up from the probe type reactor into a high throughput, high power reactor. The Nearfield™ Acoustical Processor is equipped with a 20-kilohertz (kHz) and a 16-kHz transducer (2,000 watts [W] each) that takes advantage of the effect of superposition. After testing this reactor, 17 additional 1.7-millihertz (mHz) transducers (360-W total) were added to enhance the process by increasing the generation of OH•. This reactor proved to be effective in the disinfection of both *E. coli* and *Cryptosporidium parvu*m oocysts.

15. SUBJECT TERMS
Ultrasonic water reuse, TOC, *Cryptosporidium, Giardia,* Catalytic Sonochemical Water Treatment

16. SECURITY CLASSIFICATION OF:			17. LIMITATION OF ABSTRACT	18. NUMBER OF PAGES	19a. NAME OF RESPONSIBLE PERSON
a. REPORT	b. ABSTRACT	c. THIS PAGE		80	Bob Jurenka
					19b. TELEPHONE NUMBER *(include area code)* 303-445-2254

Standard Form 298 (Rev. 8/98)
Prescribed by ANSI Std. 239-18

Desalination and Water Purification Research and Development Program Report No. 88

Treatment of Wastewaters for Water Reuse by a Catalytic Sonochemical Process – Phase II

C.P. Huang (Principal Investigator)
Pei Chiu (Co-Principal Investigator)
Samuel P. Myoda (Graduate Research Assistant)

Department of Civil and Environmental Engineering
University of Delaware

Agreement No. 99-FC-81-0184

U.S. Department of the Interior
Bureau of Reclamation
Technical Service Center
Environmental Resources Team
Water Treatment Engineering and Research Group
Denver, Colorado

May 2006

MISSION STATEMENTS

The mission of the Department of the Interior is to protect and provide access to our Nation's natural and cultural heritage and honor our trust responsibilities to Indian tribes and our commitments to island communities.

The mission of the Bureau of Reclamation is to manage, develop, and protect water and related resources in an environmentally and economically sound manner in the interest of the American public.

Disclaimer

Information contained in this report regarding commercial products or firms was supplied by those firms. It may not be used for advertising or promotional purposes and is not to be construed as an endorsement of any product or firm by the Bureau of Reclamation.

The information contained in this report was developed for the Bureau of Reclamation; no warranty as to the accuracy, usefulness, or completeness is expressed or implied.

Table of Contents

		Page
List of Acronyms		vii
Executive Summary		1
1. Enumeration of Pathogenic Protozoa		
1.1	Current Methodolgies	3
1.2	EPA Method 1623	3
1.3	Modified EPA Method 1623	4
1.3.1	Microscopic System with Dual Band Filter	6
1.4	Microscopic Examination	7
1.4.1	Staining Procedures	9
1.5	Direct Counting	11
1.6	Improved Sporozoite Staining	12
1.7	Dual Lamp Filter	13
1.8	Additional Quantification and Qualification Methods	15
1.9	Conclusions	15
2. The Nearfield™ Acoustical Processor		17
2.1	Introduction	17
2.1.1	The Nearfield™ Acoustical Processor	17
2.2	Experimental Results and Discussion	20
2.2.1	Wastewater Characterization	20
2.2.2	Particle Removal	20
2.2.3	Turbidity	24
2.2.4	TOC Removal	25
2.2.5	BOD5 Removal	25
2.2.6	Chemical Oxygen Demand Removal	28
2.2.7	*E. Coli* Disinfection	28
2.2.8	THMFP Reduction	31
2.2.9	Cryptosporidium Disinfection	33
2.3	Retention Time Calculation	33
2.3.1	Plug Flow	33
2.3.2	Tracer Tests	34
2.3.3	Dispersion Model	35
2.3.4	Ultrasonic Wave Modeling	40
2.4	Summary	40
3. The Tri-Frequency Nearfield™ Acoustical Processor		43
3.1	Introduction	43
3.2	Results and Discussion	46
3.2.1	*E. Coli* Disinfection	46
3.2.2	Cryptosporidium Disinfection	47
3.3	Conclusions	51

Table of Contents (continued)

Page

4. References 55

Appendix A: Statistical Analysis of Selective Figures 57
Appendix B: HyperTerminal Interface for Prior Automated Stage 61
Appendix C: X-keys™ Keyboard Programming 65
Appendix D: Dual Lamp Scope Housing 67
Appendix E: AutoCAD Reactor Drawings 69

List of Figures

Figure *Page*

1-1 DAPI (a) and FITC (b) Images (20X) of an Open Oocyst with Two Sporozoites 3
1-2 Sequential Examination of an Oocyst and Sporozoites Using EPA Method 1623 4
1-3 Cryptosporidium Oocysts Counted with a Hemacytometer 5
1-4 Optical Characteristics of the Dual-band Filter 7
1-5 Schematic of Microscope System 8
1-6 Olympus AX 70 Microscope, Optronics CCD Camera, and Sony Monitor 9
1-7 Well Slide Scanning Pattern 9
1-8 Cryptosporidium Oocysts with/without Sporozoites as Viewed with the Dual-band Filter 10
1-9 Slide Preparation Procedure Based on Oocyst Concentration 11
1-10 Comparison of the Quantification of Cryptosporidium Using the Hemacytometer and the Improved EPA Method 1623 12
1-11 Spectra for (a) DAPI (b) Hoechst 33342 13
1-12 Dual Lamp Spectra 13
1-13 Schematic of the Dual Lamp Setup 14
1-14 Confocal Image of *C. parvum* 15
1-15 Before and After Oocyst Images, FITC and Texas Red Cubes, Inverted Zeiss Microscope (60X) 16
2-1 Probe Reactor versus the Nearfield™ Reactor 17
2-2 The Nearfield™ NAP-3606-HP-TC Acoustical Processor 18
2-3 The Nearfield™ Reaction Chamber 18
2-4 Acoustic Pressure Wave Amplification, the Superposition of 16 and 20 kHz Frequencies 19
2-5 Schematic Diagram of the Nearfield™ Reactor 20

List of Figures (continued)

Figure		*Page*
2-6	Dead-end Filtration (a), Electric Aided Dead-end Filtration (b)	21
2-7	Cross Flow Filtration (a), Electric Field Aided Cross Flow Filtration (b)	22
2-8	*Giardia*; Zeta Potential Versus pH	23
2-9	*Cryptosporidium*; Zeta Potential Versus pH	23
2-10	Effect of Alum Addition on the Turbidity of WWTP Effluent	24
2-11	Effect of Alum Concentration (μM) on Turbidity at Various pH Values	24
2-12	Turbidity after Ultrasonic Treatment	25
2-13	The Effect of Alum Addition on TOC After Ultrasonic Treatment	26
2-14	The Effect of Ultrasound on TOC, Batch Mode	26
2-15	Ultrasonic Effects on BOD_5	27
2-16	Effect of Ultrasound on COD	28
2-17	Effect of Ultrasound on *E. coli* and Total Coliform Concentrations	29
2-18	Effect of Ultrasound on *E. coli* Concentrations	29
2-19	*E. coli* Growth Curve	30
2-20	*E. coli* Destruction, Batch Mode	31
2-21	*E. coli* Destruction with Recirculation	31
2-22	Effect of Ultrasound on THMFP	32
2-23	GC/ECD Chromatogram	32
2-24	Effect of Ultrasound on *Cryptosporidium* Concentration, Experimental Conditions; pH = 7.2, US energy intensity = 7.65W/cm^2, T = 25 ^oC	33
2-25	Tracer Test, N-NO32- Concentration at the Sampling Port	35
2-26	Tracer Test. Nitrate Concentration at Point Right After the Pump	35
2-27	Variables for a Closed Vessel in Which Reaction and Dispersion Are Occurring	36
2-28	Schematic Diagram of the Flow Pattern with Recirculation	38
2-29	Model Prediction Versus Experimental Data	39
3-1	Three Transducer Reactor Set-up	43
3-2	Rate Constants for H_2O_2 and OH• Production at Various Frequencies and Saturating Gases	44
3-3	1.7-mHz Transducer and Spacer with Embedded Transducers	45
3-4	Final Version of 1.7-mHz Transducer	46

List of Figures (continued)

Figure		*Page*
3-5	Effect of Reactor Type and Spacer Width on *E. coli* Disinfection	47
3-6	Effect of Ultrasonic Frequency on *E. coli* Disinfection	48
3-7	Effect of Spacer Width, Frequency and H_2O_2 Addition on *E. coli* Disinfection	48
3-8	Effect of Frequency and Frequency Combinations on *E. coli* Disinfection	49
3-9	*Cryptosporidium* Destruction, Tri-frequency Reactor	49
3-10	*Cryptosporidium* Destruction Versus H_2O_2 Concentration, Tri-frequency Reactor	50
3-11	Effect of a Single Frequency on *Cryptosporidium* Disinfection Using the 1¼" Tri-frequency Space	51
3-12	Effect of a Combination of Frequencies on *Cryptosporidium* Disinfection Using the 1 ¼" Tri-frequency Spacer	52
3-13	Effect of a Combination of Frequencies with H_2O_2 on *Cryptosporidium* Disinfection Using the 1 ¼" Tri-frequency Spacer	52
D-1	Dual Lamp Housing	67
E-1	Nearfield™ Reactor Schematic	69
E-2	Tri-frequency Spacer Wiring Schematic	70
E-3	Tri-frequency, 1.7 mHz-Transducers Embedded in Spacer Wall	71
E-4	Overview of Tri-frequency Placement Within Nearfield™ Reactor	72

List of Tables

Table		*Page*
2-1	Wastewater Characterization	21
3-1	Compression Half-cycle Length, Bubble Collapse Time, and Resonant Bubble Radii for Ar and Kr as Saturating Gases	44

List of Acronyms

BrdU	Bromodeoxyuridine
C	degree Celsius
cm^2	square centimeter
DAPI	Diamidino Phenylinodole
DABCO	diazabicyclo-octane
DIC	differential interference contrast
DBP	disinfection by-product
ds	double stranded
ECD	electron capture detector
EI	electron impact
EPA	Enviromental Protection Agency
E. coli	*Escherichia coli*
FITC	fluorescein isothiocyanate
gpm	gallons per minute
Hz	Hertz
IMS	immunomagnetic separation
ICP	inductively coupled plasma
kHz	Kilohertz
L	Liter
mHz	Megahertz
°L	Microliter
µM	Micrometer
mHz	Millihertz
min	Minute
mL	Milliliter
mm	Millimeter
PBS	phosphate buffer solution
PCR	polymerase chain reaction
pH	hydrogen-ion concentration
RF	reistor-faraday
THMPF	trihalomethane formation potential
TOC	total organic carbon
UV	Ultraviolet
V	Volts
WWTP	waste water treatment plant
W	Watt

Executive Summary

The second year of the project, "Waste Water Reuse by a Catalytic Sonochemical Process," was spent designing and refining a pilot plant scale reactor that could efficiently and cost effectively take advantage of the capabilities of the ultrasonic process to disinfect and oxidize the organic contaminants typically found in waste water effluent. In addition to completing work on the reactor, the modified qualification and quantification methodology based on EPA Method 1623 for *Cryptosporidium parvum* was finalized.

The prototype of the dual filter set was improved to include a second lamp so that simultaneous ultraviolet (UV) and visible light excitation is possible. Using this setup, Fluorescein (FITC) labeled oocysts and 4', 6-diamidino-2-phenylindole (DAPI) or Hoechst 33342 stained sporozoites can be viewed at the same time, substantially reducing analysis time and improving accuracy.

A Nearfield™ Acoustical Processor was purchased to scale up from the probe type reactor into a high throughput, high power reactor. The Nearfield™ Acoustical Processor is equipped with a 20 kHz and a 16 kHz transducer (2,000 W each) that takes advantage of the effect of superposition. After testing this reactor, 17 additional 1.7 mHz transducers (360 W total) were added to enhance the process by increasing the generation of OH•. This reactor proved to be effective in the disinfection of both *Escherichia coli (E. coli)* and *Cryptosporidium parvum* oocysts.

1. Enumeration of Pathogenic Protozoa

1.1 Current Methodologies

The qualification and quantification of viable *Cryptosporidium* oocysts has been a problem for the water supply and resource industry. Much effort has been made to develop an accurate, inexpensive, sensitive, and simple method to detect viable oocysts in water supplies. These approaches include flow cytometry (Vesey et al., 1993), polymerase chain reaction (PCR) methods (Webster et al., 1993), electrorotation (Beardsley, T., 1993), enzyme-linked immunosorbent assay (ELISA) (Chapman et al., 1990), turbidity correlation, colorimetric methods and cultural methods (Upton et al., 1994). Despite advances in all of these approaches, the most reliable and widely accepted method is immunofluorescence. Currently, EPA Method 1623 is the standard for the quantification and qualification of *Cryptosporidium* and *Giardia*. Although effective, it is time consuming and does not directly measure viability. Oocysts that contain sporozoites are assumed viable (oocysts are a protective housing for the sporozoites that will infect the host). This results in an overestimation of the actual number of viable oocysts.

1.2 EPA Method 1623

EPA Method 1623 utilizes filtration to concentrate the oocysts and cysts, immunomagnetic separation to remove them from other particulate matter, Fluorescein (FITC) labeled antibodies to label the oocysts and cysts, and 4', 6-diamidino-2-phenylindole (DAPI) staining of the sporozoites in preparation for microscopic examination. Using both FITC and DAPI filter cubes, the oocysts and sporozoites are evaluated (figure 1-1, a, b). The oocyst is first located using visible light to excite the fluorescent antibody on the oocyst and then ultraviolet (UV) light to excite the nucleic acid staining within the sporozoites. This requires

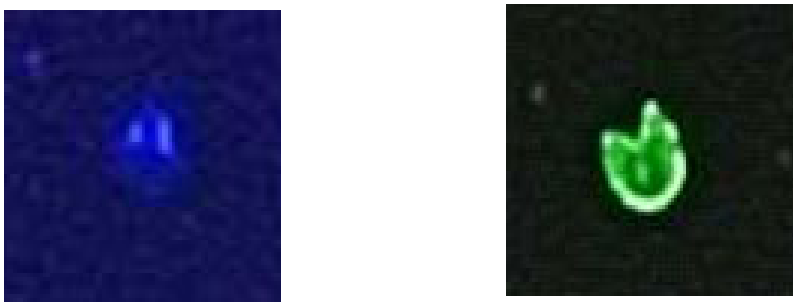

(a) (b)

Figure 1-1 – DAPI (a) and FITC (b) Images (20X) of an Open Oocyst with Two Sporozoites.

a change of the microscope's filter each time an oocyst is located. The oocyst and sporozoite images cannot be viewed simultaneously so the location of the sporozoites relative to the oocyst can not be verified.

Figure 1-2 represents images viewed according to EPA Method 1623. The first step is to locate a FITC (green) labeled oocyst (a), next the filter set is changed over to DAPI (blue) to verify if sporozoites are present within the located oocyst (b). Without analyzing both images together it is hard to determine if the sporozoites are truly in the oocyst. Image (c) illustrates their relative positions. That is, according to EPA Method 1623, it is likely that a sporozoite can be located outside of an oocyst and not be counted.

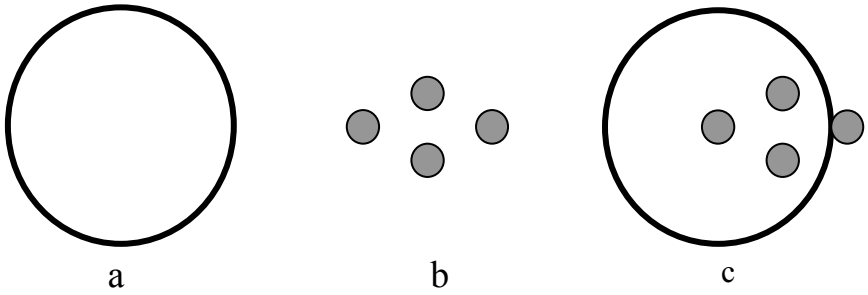

Figure 1-2 – Sequential Examination of an Oocyst and Sporozoites Using EPA Method 1623.

1.3 Modified EPA Method 1623

The method we will used to quantify Cryptosporidium is based on EPA Method 1622: *Cryptosporidium* in Water by Filtration/IMS/FA (September 1998). Water samples are filtered and the oocysts and extraneous materials are retained on the filter. The materials on the filter are removed by elution with an aqueous buffered salt and detergent solution. The salt/detergent solution from the filter is centrifuged to settle the oocysts, and the supernatant is decanted. (This step is omitted when sample volumes are relatively small and the oocyst concentrations are relatively high). The oocysts are magnetized by attachment of magnetic beads conjugated to an antibody. The magnetized oocysts are separated from the extraneous material using a magnet, and the extraneous materials are discarded. The magnetic bead complex is then detached from the oocysts.

The oocysts are stained on well slides with fluorescently labeled monoclonal antibodies and vital dye. The stained sample is examined using fluorescence and differential interference contrast (DIC) microscopy. Scanning each slide well for objects that meet the size, shape, and fluorescence characteristics of *Cryptosporidium* oocysts performs qualitative analysis. Potential oocysts are confirmed through 4', DAPI vital dye-staining characteristics and

DIC microscopy. An oocyst is identified when size, shape, color and morphology agree with specified criteria and examples in a photographic library. The total number of objects on the slides confirmed as oocysts will reflect the oocyst concentration in the initial volume of the sample. Quality is assured through reproducible calibration and testing of the filtration, immunomagnetic separation (IMS), staining, and microscopy systems.

The first step in developing this procedure was to ensure high oocyst recovery percentages from purified oocyst samples suspended in distilled water. Because no extraneous material was present in these suspensions, the filtration and staining steps were omitted and the oocysts were counted using a hemacytometer (figure 1-3). Oocyst recovery was calculated based on the following formula:

$$R = 100\frac{N_{sp} - N_s}{T} \tag{3.1}$$

where: R = % recovery
N_{sp} = # oocysts detected in the spiked sample
N_s = # oocysts detected in unspiked sample
T = true value of oocysts spiked

The R value in these tests was 87 ± 5 percent. Recovery percentages in samples spiked in waste water that underwent the complete identification and detection method have been a little lower. These values, as well as a protozoa library of color photographs of *Cryptosporidium* oocysts and any interfering organisms and/or debris by FA and DAPI, were developed.

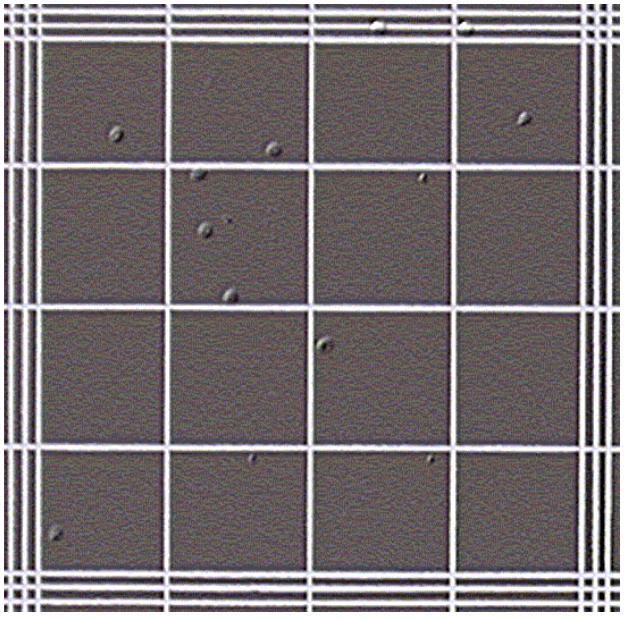

Figure 1-3 – *Cryptosporidium* Oocysts Counted with a Hemacytometer.

1.3.1 Microscopic System with Dual Band Filter

Developing a system that would allow the simultaneous viewing of the oocyst and sporozoites would improve the accuracy in assessing the position of the sporozoites relative to the oocysts. It would also allow one to see any sporozoites that have been released or are in oocysts that were not labeled. A more accurate count would be realized. In addition, because the filters need be changed each time an oocyst is located, the evaluation time would be cut by approximately 60 percent.

Commercially available dual band filter cube sets that allow the simultaneous viewing of the FITC and DAPI labeled samples were tested and were found to be ineffective. Upon closer inspection of their characteristic curves (transmission ratio (percent) versus wavelength (nm)), it was determined that they were designed for the high DAPI and low FITC concentrations typical of most biological samples. *Cryptosporidium* has exactly the opposite characteristics—high FITC and low DAPI concentrations. The FITC signal overwhelms the DAPI signal and the sporozoites can not be detected. A filter cube that will reduce the FITC signal without limiting the DAPI signal was designed.

A filter cube consists of three components: the barrier filter, dichroic mirror, and excitation filter. The filter cube is housed in the cube cassette located above the objective lens turret. After identifying the general shapes of the characteristic curves of the filters needed, a variety of cube configurations were tested. The final combination arrived at was the barrier filter and excitation filter from a wide band UV filter coupled with a dichroic mirror from a dual band DAPI/FITC cube set. The wide band UV components let both the FITC and DAPI signal through, and the dichroic mirror provides improved differentiation between blue and green (figure 1-4) compared to a wide band dichroic mirror. The excitation filter allows light between 305 and 390 nm through (absorbed by the DAPI) with enough bleed through at higher wavelengths to excite the FITC. This custom cube significantly reduces the strength of the FITC signal to allow the simultaneous viewing of oocysts and sporozoites.

Other deviations in our methodology from EPA Method 1623 include the way in which the cysts, oocysts, and sporozoites are microscopically observed. Instead of viewing the slide through the eyepiece, an Olympus AX 70 microscope equipped with an Optronics CCD camera and Sony monitor is used. Figure 1-5 illustrates a schematic, and figure 1-6 is a picture of our system.

This system allows viewing the image in a larger format, making evaluation much easier. The monitor screen represents one grid on the well slide, eliminating the overlap associated with viewing rectangular grids within a circular field. We have taken our improvement of the system further by installing a Prior motorized stage and a X-keys (Tiger Direct, #P55-2000) 16 key programmable keyboard. The stage is connected to the computer via a serial port and its movement is

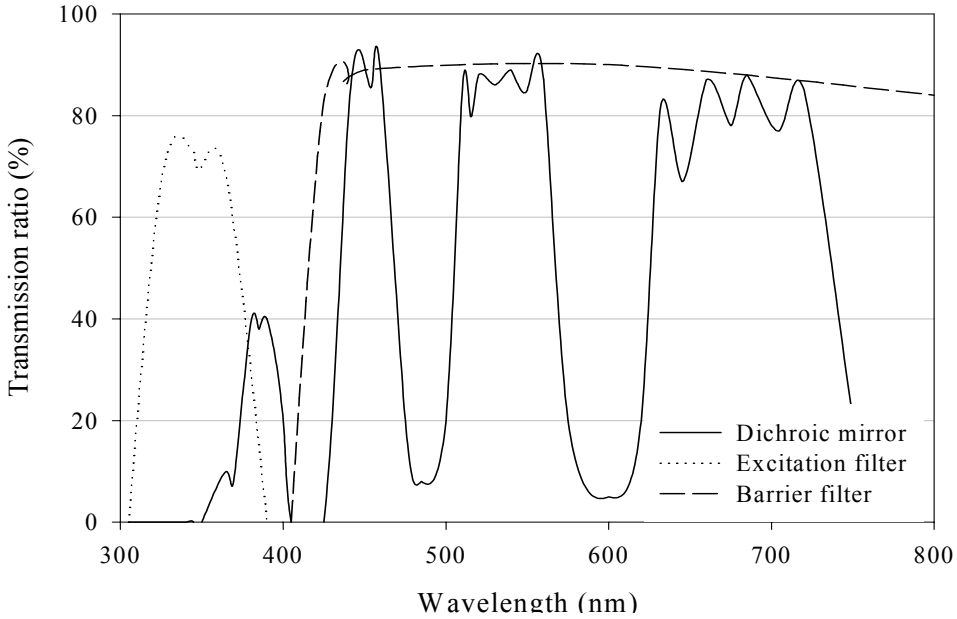

Figure 1-4 – Optical Characteristics of the Dual-band Filter.

controlled using a HyperTerminal interface. The X-keys keyboard is programmed so that single key strokes replace the string of keystrokes required to precisely control the stage movement up, down, left, and right, eliminating the error associated with manually moving the stage. A preset raster or snake pattern can also be input using single keys. In addition, the computer controls the stage z position (focus). The HyperTerminal command strings are included with the Prior stage and the instructions to convert these strings into single keystrokes are included with the X-Keys keyboard. The relative position of the slide is displayed on the computer monitor so that the location of any object that may require further evaluation may be recorded. These improvements allow the examination of well slides in a quick and efficient manner while ensuring 100-percent coverage without any over- or under-lapping that would result in too high or low oocyst counts.

1.4 Microscopic Examination

Slides were examined using an Olympus AX70 microscope with 20, 40, and 100X oil objective lenses connected to an Optronics CCD camera and Sony color monitor. Each well slide was scanned following the pattern represented in figure 1-7. Using a FITC cube with a fluorescent light source, oocysts appeared as brilliant apple-green spherical objects 4 to 6 μm in diameter with bright-lighted edges. After an oocyst was located, the FITC cube was replaced by a DAPI cube and evaluated for sporozoites. DAPI staining of sporozoites exhibited up to four

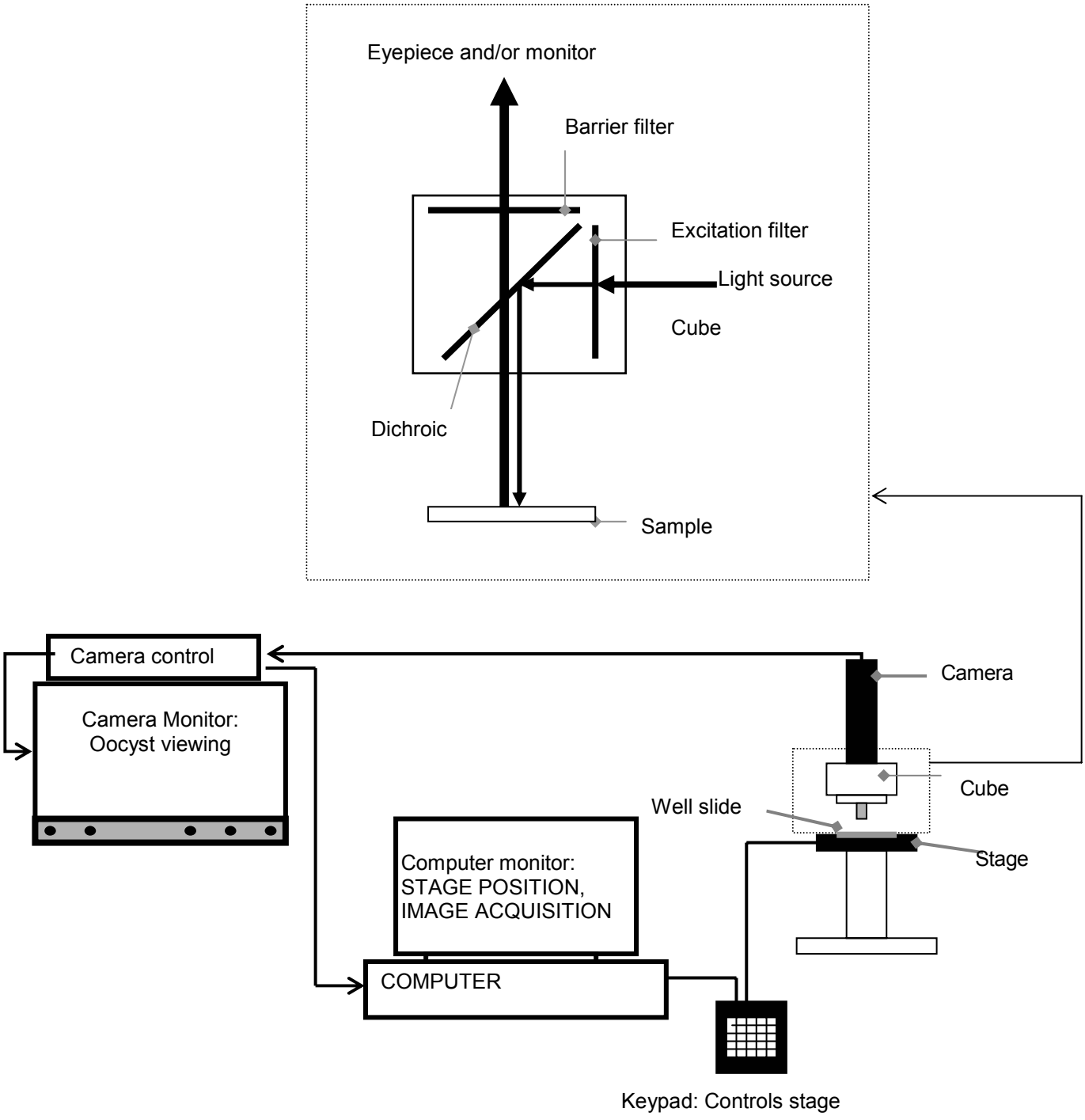

Figure 1-5 – Schematic of Microscope System.

Figure 1-6 – Olympus AX 70 Microscope, Optronics CCD Camera, and Sony Monitor.

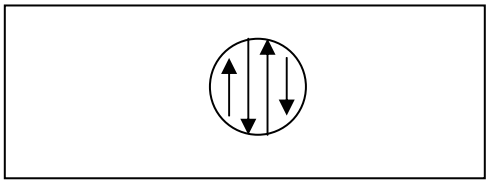

Figure 1-7 – Well Slide Scanning Pattern.

sky-blue nuclei and/or intense blue internal staining. Oocysts exhibiting both these characteristics were counted as viable oocysts. It was interesting to note that virtually all (88-100 percent) of the oocysts that exhibited the characteristic brilliant apple-green spherical shape with highlighted edges contained sporozoites in samples that had undergone at least a 1 $\log_{10}$ removal by ultrasound.

Figure 1-7 shows the raster pattern according to which way the well slides are scanned.

Figure 1-8 shows *Cryptosporidium* Oocyst images as viewed with the dual-band filter. These three images illustrate oocysts both with and without sporozoites. Image (a) is a cluster of oocysts with seven containing sporozoites and four empty. Image (b) illustrates two full and one empty oocyst and image (c) shows one empty and one full oocyst. It would be virtually impossible to determine which oocysts contain sporozoites without viewing the FITC and DAPI image simultaneously.

1.4.1 Staining Procedures

For samples with an estimated oocyst concentration between 10^4-10^5 oocysts me per milliliter (/mL), a 1-mL aliquot of the sample to be analyzed was diluted with

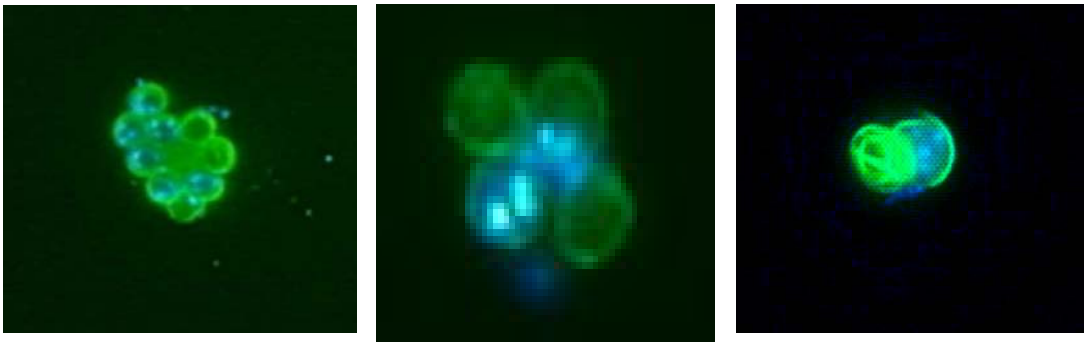

a. b. c.

Figure 1-8 – *Cryptosporidium* Oocysts with/without Sporozoites as Viewed with the Dual-band Filter.

9 mL of distilled, deionized (reagent) water. After vortexing for at least 2 minutes, 50 µL of this dilution was overlaid on a Dynal 9 mm well slide and dried in an incubator for ~1 hour at 42 °C. After drying, 40 µL of absolute methanol was applied to the slide and allowed to air dry for ~10 minutes. After that time, 50 µL of 1X Waterborne A400FL Crypto-a-Glo (Mab) was applied to the slide. The slides were placed on a rack over wet paper towels in a sealed plastic container (humid chamber) and incubated at 37 °C for 30 minutes. The excess Mab was aspirated with disposable transfer pipettes and washed three times with a 150 mM phosphate buffer solution (PBS). Next, 50 µL of 4',6-diamidino-2-phenylindole (DAPI) staining solution was applied and allowed to stand for ~10 minutes. The slide was then washed three more times with PBS and once with reagent water. After drying at 37 °C in an incubator on a rack over desiccant in a sealed plastic container (dry box), 6 µL of 2 percent 1,4-diazabicyclo-[2.2.2]octane (DABCO) mounting media (78 percent glycerol, 22 percent water) was applied. After drying, a cover slip was installed and sealed with clear nail polish. Slides were stored in a dry box in the dark prior to microscopic examination.

Samples that had an estimated oocyst concentration between 10^3-10^4 oocysts/mL (figure 1-9) were prepared following the above procedure with the following exception; the initial 1-mL sample was not diluted with 9 mL of reagent water.

Samples that had an estimated oocyst concentration $<10^3$ oocysts/mL were concentrated via immunomagnetic separation prior to slide preparation. A 0.5-mL sample was added to 9.5 mL reagent water in a Dynal L10 tube containing 1 mL 10X SL buffer A and 1 mL 10X SL buffer B. 100 µL of vortexed Dynabeads anti-*Cryptosporidium* beads were added and the tube was rotated on a Dynal sample mixer for 1 hour. The L10 tubes were then removed from the mixer and placed in Dynal MPC-1 magnetic concentrators and gently rocked for 1 minute. The supernatant was then decanted, the magnet removed,

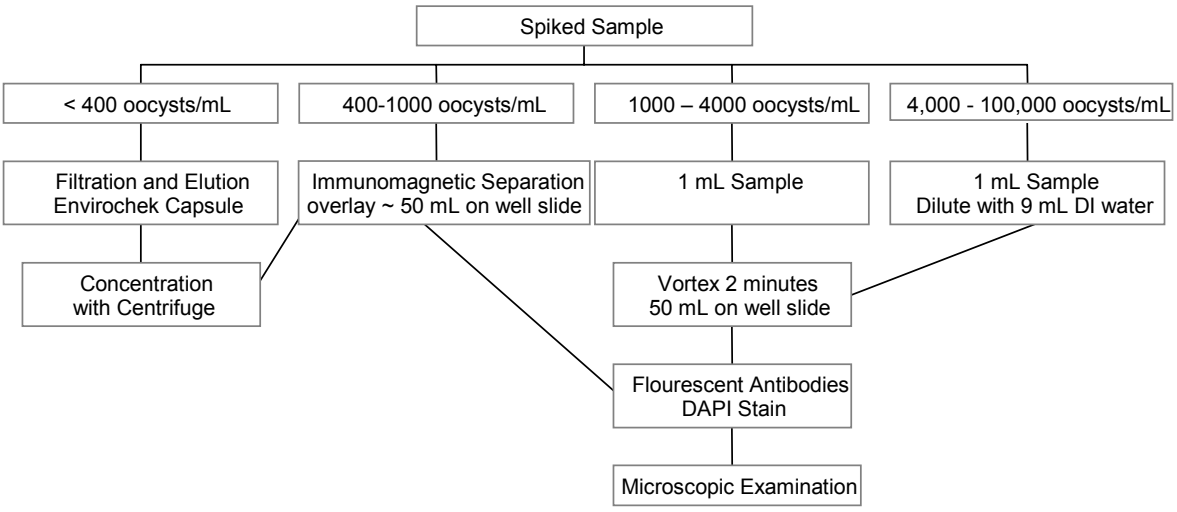

Figure 1-9 – Slide Preparation Procedure Based on Oocyst Concentration.

and the oocyst/bead complexes were resuspended in 1 mL 1X SL buffer A. This suspension was then transferred into a 1.5-mL Eppendorf tube. The tube was placed in a Dynal MPC-M magnet and gently rocked for 1 minute. The supernatant was immediately aspirated and the MPC-M magnetic strip was removed. HCl (50 µL, 0.1N) was added and the tube was vortexed for 5 seconds. After standing for 5 minutes in the MPC-M, the tubes were again vortexed for 5 seconds and put back in the MPC-M with the magnetic strip in place. NaOH (5 µL, 1N) was placed on the well slide and all the fluid from the Eppendorf tube was transferred onto the slide. The slide preparation and staining procedures following these steps were the same as mentioned above.

Positive and negative controls were analyzed with each sample series. Positive controls were prepared by pipetting 10 µL of positive antigen onto ~ 500 oocysts on well slide. Negative controls were prepared by adding 75 µL of PBS on a well slide. The slides were then stained following the methodology described previously.

1.5 Direct Counting

In order to compare the modified Method 1623 with a direct counting method, a hemacytometer was used to quantify oocyst concentrations in both the spiked waste water and distilled-deionized water samples (a large portion of the empty oocysts in these samples had been destroyed prior to this analysis - Huang et al., 2000). Ten µL of sample were loaded in each chamber of the hemacytometer, and the total number of oocysts present in four 1-mm^2 areas was recorded. Six hemacytometer counts were used for each sample (a total of twenty-four 1-mm^2 areas were averaged to determine the oocyst concentration).

Figure 1-10 shows the comparison of the hemacytometer counts with the modified Method 1623 in both the distilled-deionized water and the waste water. The error bars represent standard deviation. In both cases the hemacytometer count was higher than the modified Method 1623 count, reflecting the inability to differentiate oocysts containing sporozoites versus empty oocysts resulting in overestimation by the hemacytometer method. There was a greater difference in hemacytometer versus modified Method 1623 counts in the samples that were spiked in waste water. This is probably due to interference by components within the waste water that inhibit the fluorescent labeling of the oocysts.

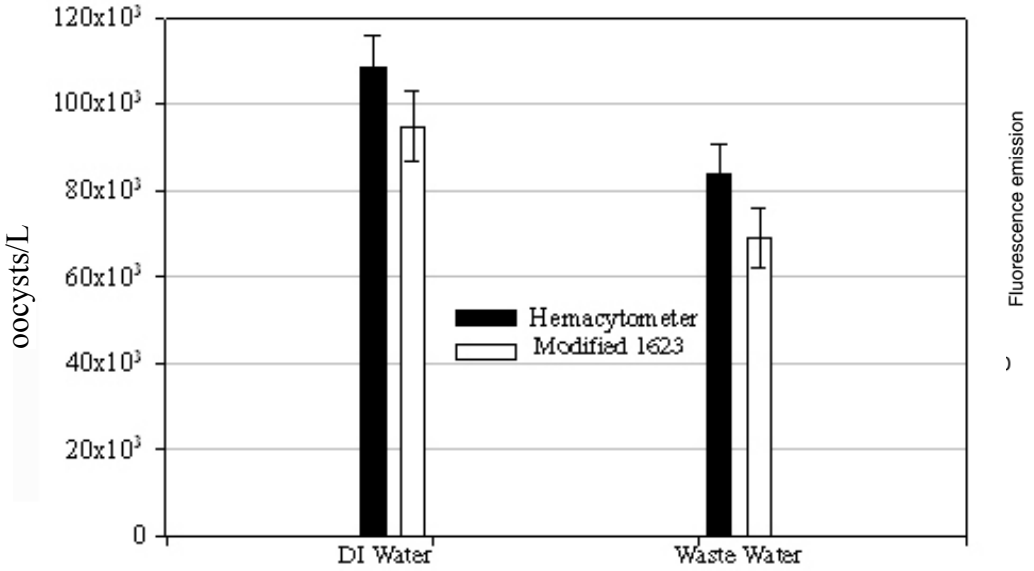

Figure 1-10 – Comparison of the Quantification of *Cryptosporidium* Using the Hemacytometer and the Improved EPA Method 1623.

1.6 Improved Sporozoite Staining

Hoechst 33342 dye has been used in place of DAPI to stain the sporozoites in order to intensify the blue emissions so even greater separation between the blue sporozoites and green (FITC labeled) oocyst can be achieved.

DAPI is the classic nuclear and chromosome counterstain, used for years to identify nuclei and show chromosome-banding patterns. DAPI binds selectively to double stranded DNA (dsDNA) and thus shows little to no background staining of the cytoplasm. Its relatively low-level fluorescence emission does not overwhelm signals from green- or red-fluorescent secondary antibodies. This low emission dictated the development of the dual filter set currently being used.

The Hoechst 33342 dye has been widely used for staining the nuclei of living cells. Hoechst dyes preferentially bind to aidinine-thymine (AT) regions, making

them quite selective for DNA; Hoechst dye–stained cells and tissues show virtually no cytoplasmic staining. Hoechst 33342 is commonly used in combination with bromodeoxyuridine (BrdU) to distinguish the compact chromatin of apoptotic nuclei, to identify replicating cells and to sort cells based on their DNA content. The Hoechst 33342 dye has a much higher fluorescence emission than the DAPI, making it a better choice for the dual labeled *Cryptosporidium* samples. Figure 1-11 illustrates the spectra of the two dyes.

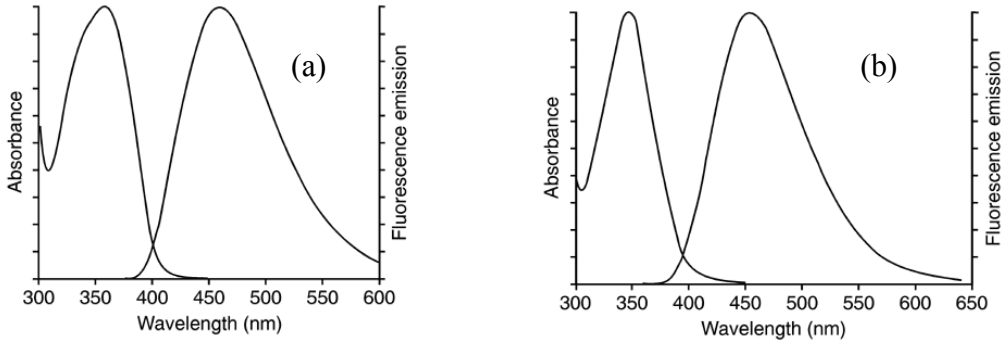

Figure 1-11 – Spectra for (a) DAPI (b) Hoechst 33342.

1.7 Dual Lamp Filter

To improve the dual band filter spectra, a dual lamp system was developed to increase the UV excitation and eliminate the need for digital image enhancement. The addition of the second lamp allows simultaneous UV and visible light excitation while eliminating the absorption/reflection of light associated with traditional dual excitation filters. Figure 1-12 illustrates the final spectra of the dual lamp setup and figure 1-13 is the schematic of the dual lamp system. True UV and visible light excitation is achieved.

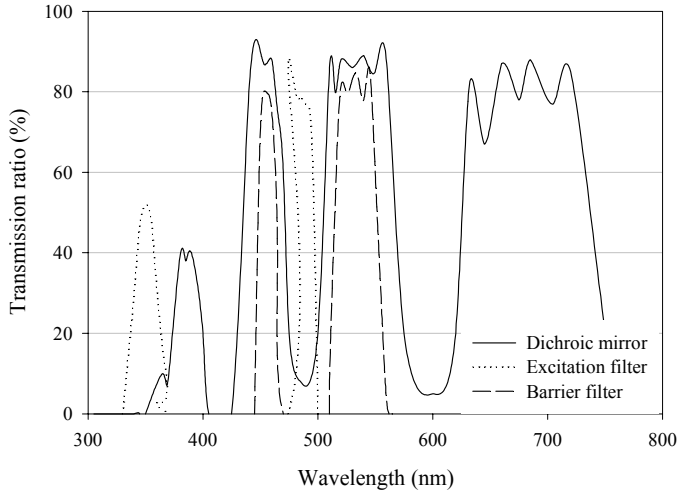

Figure 1-12 – Dual Lamp Spectra.

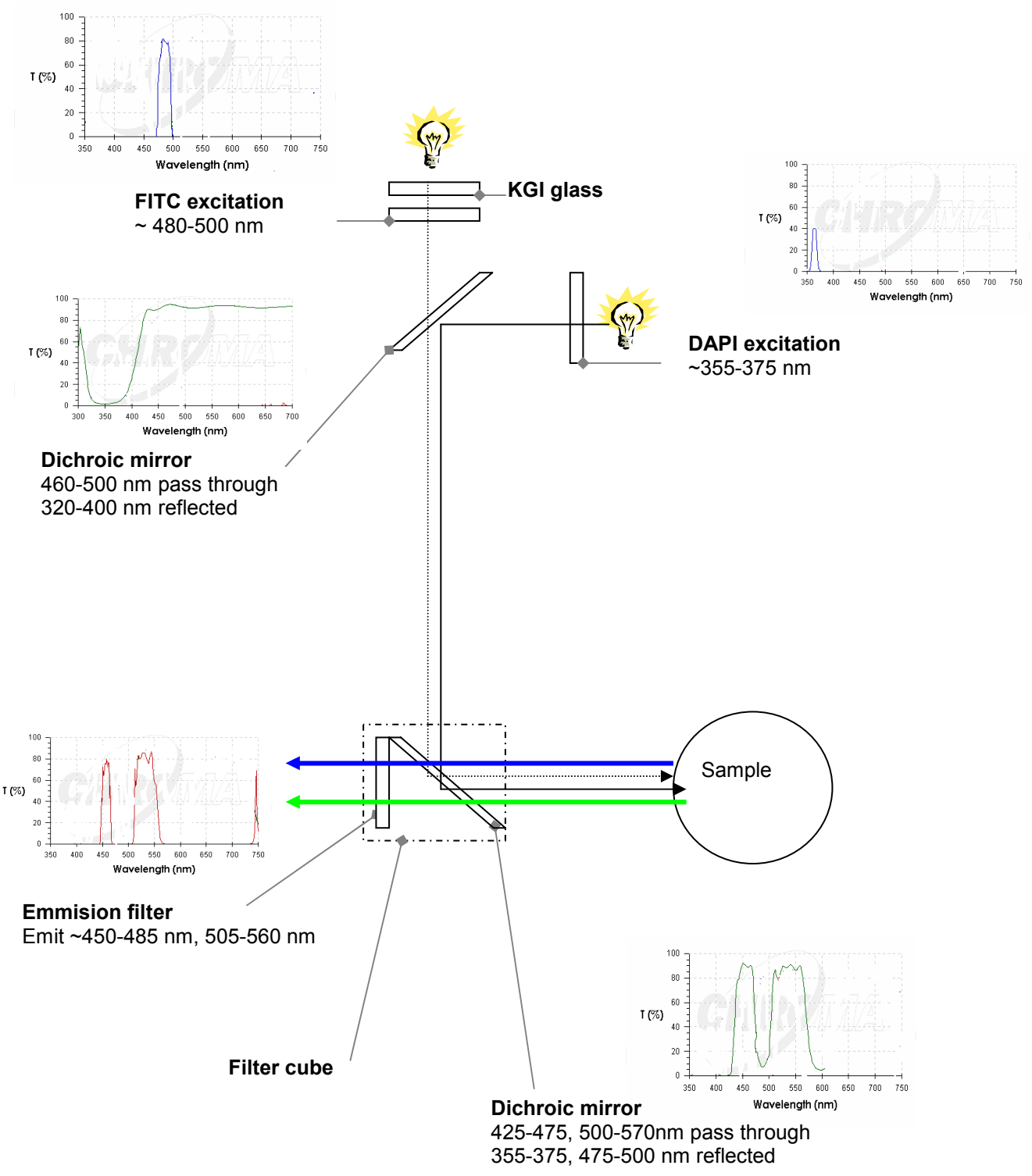

Figure 1-13 – Schematic of the Dual Lamp Setup.

1.8 Additional Quantification and Qualification Methods

In addition to the immunoflourescent method, the polymerase chain reaction (PCR) outlined by Johnson et al., 1995 and confocal microscopy have been employed. The PCR procedure has been preformed using two different pairs of primers: 5'- AAGCTCGTAGTTGGATTTCTG-3', 5'-TAAGGTGCTGAAGGAGTAAGG-3' and 5'-AGCAATCCTCTGCCGTACAGG-3', 5'-AAGAGCATCCTTGATCTTCT-3'. The first pair of primers produces a 435-bp product and the second pair produces a 590-bp product. These primers were obtained from the Great American Gene Company. Various methods of DNA extraction were tried, the best seemed to be following the freeze-thaw method from Stinear et al., 1996. Centrifuge 1 mL of spiked samples at 5,000 x g for 3 minutes to pellet oocysts, and resuspend in 200 :l of Bio-Rad InstaGene matrix, then vortex. After the pellet was resuspended, add 200 :l of lysis-binding buffer and subject the sample to five cycles of freezing in liquid nitrogen for one minute and thawing at 65 °C for 1 minute.

Confocal microscopy has also been used to explore the effects of the ultrasonic treatment. Figure 1-14 represents a section of a z-series taken of an oocyst. An oocyst image taken with the confocal microscope both before and after subjected to 40 W/ for 30 seconds, pH 7.8. We have made minor modifications to our ultrasound apparatus, designed a teflon and glass well slide and have been able to capture video of the effects of ultrasound on the oocysts. Texas Red was used instead of DAPI stain (confocal didn't have DAPI cube set) and the ultrasonic generator was placed in the well slide. Vectabond held oocysts in place on the well slide during filming (figure 1-15).

1.9 Conclusions

The automated microscope stage combined with the external monitor provided significant improvements with regard to the ease, analysis time, and accuracy as compared to eyepiece viewing and manual stage movement. Images acquired

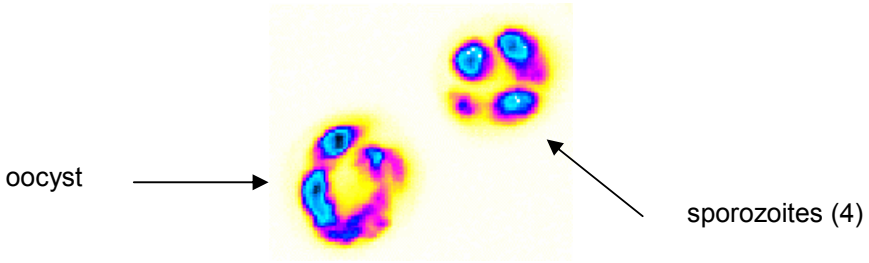

Figure 1-14 – Confocal Image of *C. parvum*.

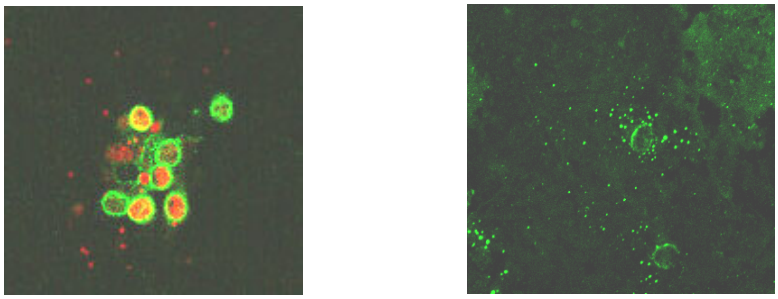

(a) (b)

Figure 1-15 – Before and after Oocyst Images, FITC and Texas Red cubes, inverted Zeiss microscope (60X).

using a 40x oil immersion lens were magnified an additional 2.5x prior to being displayed on the monitor. The large format of these images made quantification and qualification much easier. Controlling the stage with the computer ensured that no areas of the well slide would be counted twice or missed. The coordinates of any image on the slide could be recorded for future reevaluation.

The newly designed dual band filter set allows the simultaneous viewing of both FITC and DAPI labeled samples so that *Cryptosporidium* oocysts and sporozoites could be viewed together. The use of this filter instead of separate FITC and DAPI filter sets greatly reduced analysis time and provided much better spatial data with regard to the position of the sporozoites relative to the oocysts. Figure 1-8 illustrated how easily sporozoite containing oocyst concentrations can be overestimated by methods that cannot differentiate between oocysts that contain sporozoites and those that are empty. Analysis of a variety of samples revealed that between 53 percent and 88 percent of the oocysts contain sporozoites (Huang et al., 2000). At a minimum, this cube set can be used in place of the DAPI filter cube set to provide the relative positioning.

The dual lamp system completely overcomes the problem of simultaneous UV and visible light excitation, allowing even better FITC and DAPI imaging than the dual filter system. The dual lamp setup can be used for any imaging that requires UV and visible light excitation.

The original FITC and DAPI cubes were left on the microscope so images that could not be positively identified could be compared to images captured following EPA Method 1623. These comparisons help further develop the reliability of the modified method. DIC microscopy was also used to confirm oocyst qualification during method development.

2. The Nearfield™ Acoustical Processor

2.1 Introduction

As reported in the first year of this project, the probe type sonochemical reactor was used to demonstrate the feasibility of the sonochemical process. Obviously, this is an energy intensive reactor. A great deal of the acoustical energy is lost through the glass reactor. Also, there are many "dead" zones within the reactor because the acoustical waves are directional (figure 2-1). In order to eliminate these problems, a stainless steel commercial reactor was utilized.

2.1.1 The Nearfield™ Processor

A Nearfield™ NAP-3606-HP-TC Acoustical Processor was purchased from Advanced Sonic Processing Systems, Oxford, CT (figure 2-2) to demonstrate both the technical and financial feasibility of the ultrasonic process in pilot and treatment plant scales. This reactor is equipped with two 2,000 W transducers (16 kHz and 20 kHz) and is capable of treating a maximum flow rate of 15 gal/minute. Figure 2-3 shows the cross sectional details of the reactor layout.

In addition to the benefits realized by increased power and physical layout that ensure there are no "dead" areas within the reactor, the interaction between the two different frequencies doubles the relative pressure amplitude produced by either the 16 kHz or 20 kHz waves individually. The large pressure differential between the high and low pressure zones create intense implosive forces within the processing chamber. Figure 2-4 illustrates the acoustic pressure wave amplification.

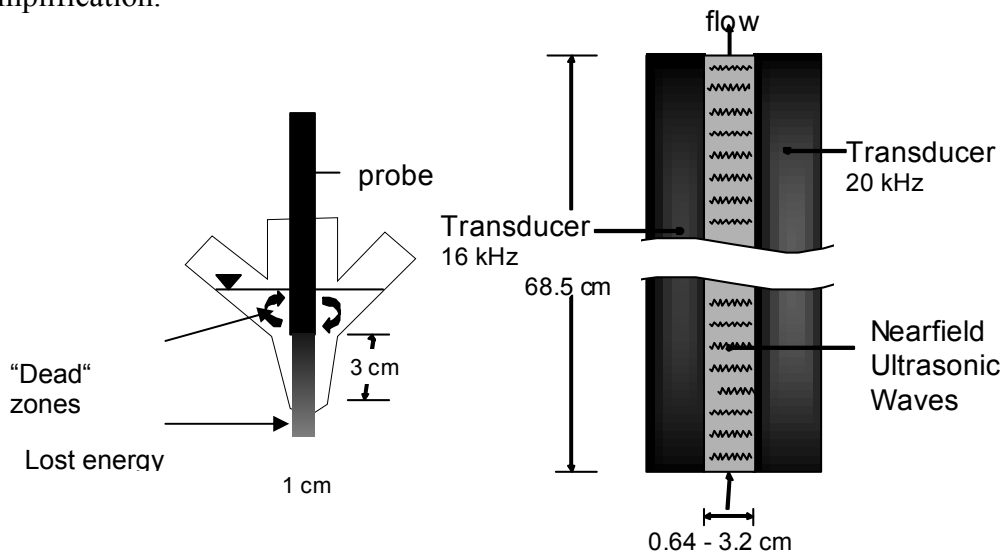

Figure 2-1 – Probe Reactor versus the Nearfield™ Reactor.

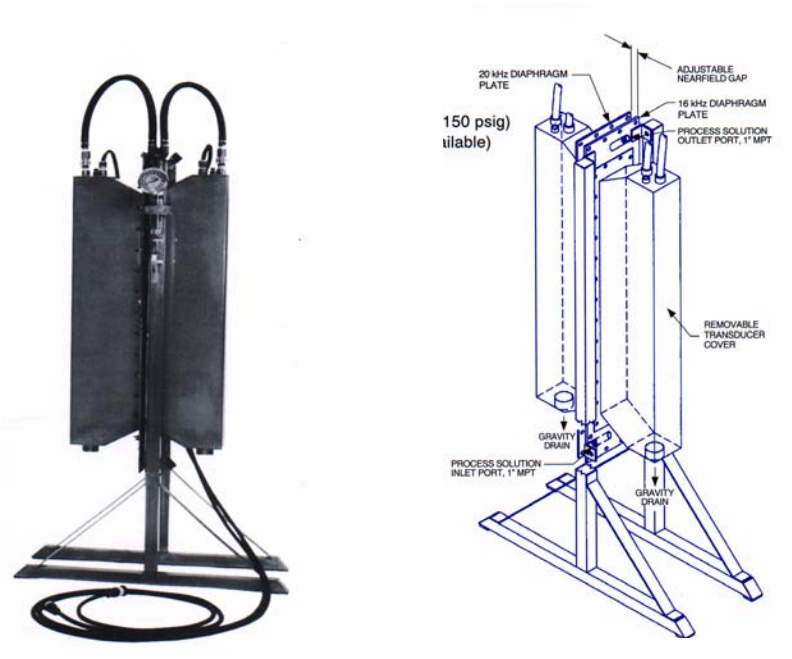

Figure 2-2 – The Nearfield™ NAP-3606-HP-TC Acoustical Processor.

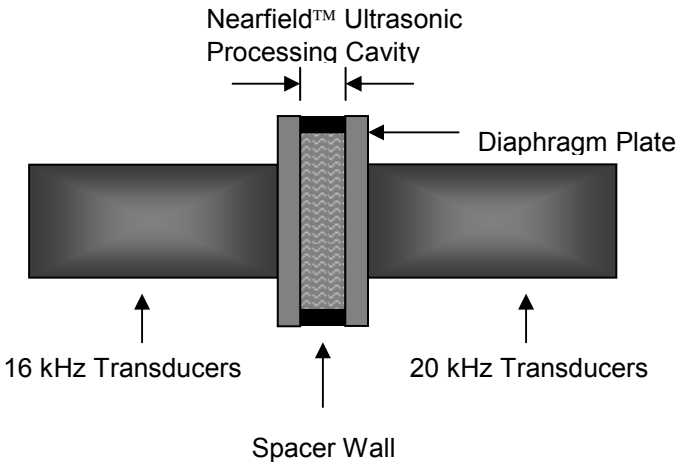

Figure 2-3 – The Nearfield™ Reaction Chamber.

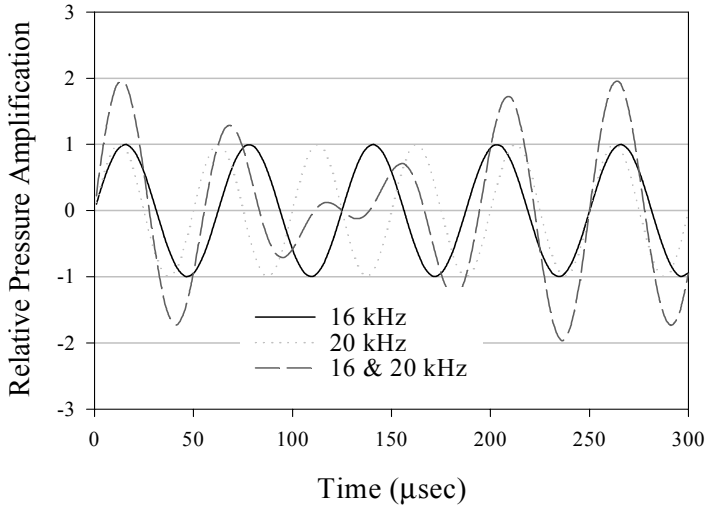

Figure 2-4 – Acoustic Pressure Wave Amplification, the Superposition of 16 and 20 kHz Frequencies.

The Nearfield™ reactor set up is shown in figure 2-5. A spiked sample was loaded into the sample container and was kept homogeneous with a magnetic stirrer. The sample was then pumped (12-V, 2.5-gpm marine pump) up into the reaction chamber and subjected to the ultrasonic waves. After treatment, the sample could either be drawn out of the sample port for analysis, discarded via the waste stream into the sink, or recycled back into the sample container for further treatment. The temperature of the reactor was controlled using cold water flowing down through the transducers and into the cooling water bucket. It is important not to allow any back-pressure to build up in the transducers so that energy is not absorbed by the cooling water. To facilitate this, a float switch and pump (12-V, marine switch and bilge pump) were installed to drain the cooling water bucket into the sink before it could fill up over the cooling water inlet. The reactor was equipped with drain valves to flush the system, and the generators were plugged into separate 20 amp circuits.

Initially, PVC pipe (½") was incorporated in the reactor design to deliver, circulate, and draw samples. The piping configuration has been redesigned using stainless steel tubing (¼") and a three-way solenoid valve has been added. Reducing the tube diameter decreases the total volume of sample within the processor from ~2.4 L to <1 L, significantly reducing material costs, specifically Cryptosporidium and Giardia culture costs. Replacing the manual ball valve with the three-way solenoid valve serves two purposes. First, it eliminates the dead space in the T-union just prior to the valve that solid material could accumulate in. Second, it allows us to automate the sampling port. The three-way solenoid valve is connected to a fractional collector so that precise timing and sample volume can be maintained.

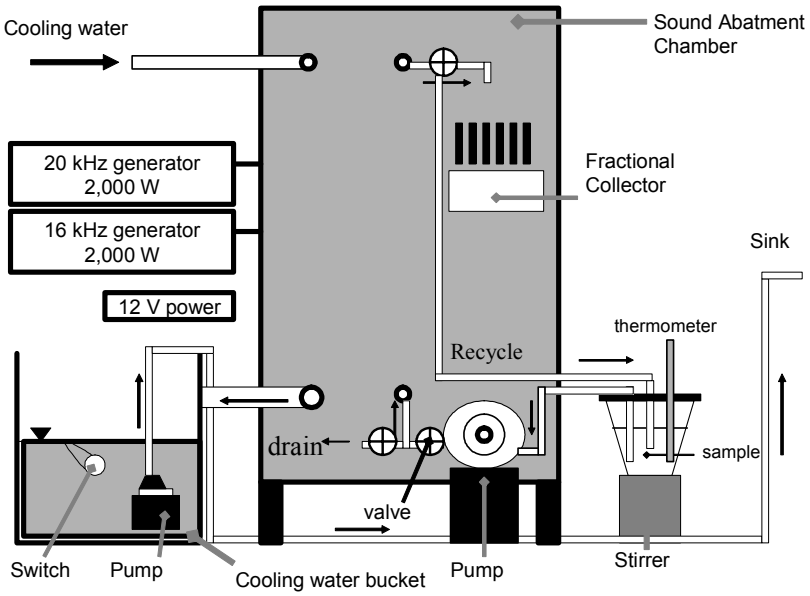

Figure 2-5 – Schematic Diagram of the Nearfield™ Reactor.

2.2 Experimental Results and Discussion

2.2.1 Waste Water Characterization

Grab samples were periodically taken from the Wilmington Waste Water Treatment Plant (WWTP), the Blue Plains Waste Water Treatment Plant (BPWTP), and the Little Pawtuxet Waste Water Treatment Plant (LPWTP). The Na, Mg (II), K, Ca (II), Mn (II), and Fe (II) contents were evaluated by inductively coupled plasma (ICP) following method 3120 (metals by plasma emission spectroscopy) as described in *Standard Methods for the Examination of Water and Wastewater*, 19th edition, 1995. Typical results of this analysis are shown in table 2-1. Also reflected in this table are the pH and alkalinity values. The alkalinity value was calculated using the titration method (method 2320 B) and the pH value was calculated using the electrometric method (method 4500-H+ B). These procedures are outlined in the 18th edition of *Standard Methods for the Examination of Water and Wastewater* (1992).

2.2.2 Particle Removal

The majority of the waste water samples were filtered before experiments were carried out. This was done primarily to minimize interference when staining the *Cryptosporidium* oocysts. In previously reported THMFP reduction experiments, there seemed to be an initial increase in formation potential before it decreased. We speculate that this may be caused by the break up of large macro-molecules

Table 2-1 – Waste Water Characterization

Characteristics	WWTP	BPWTP	LPWTP
PH	7.13	6.51	6.92
Na(I) (ppm)	74.30	34.75	8.94
Mg(II) (ppm)	11.76	5.82	5.94
K(I) (ppm)	14.27	8.95	10.71
Ca(II) (ppm)	28.05	30.82	30.67
Mn(II) (ppb)	152.5	108.9	29.7
Fe(II) (ppb)	87.6	48.12	18.2
Alkalinity (mg-$CaCO_3$/L)	183	43	83

into smaller molecules that are more active DBP precursors. In an effort to test this theory we have pursued two different strategies. The first is to test filtered and unfiltered effluent and determine if the initial concentration increases, decreases or is eliminated. A major drawback to this approach is the amount of time required to filter an adequate volume of sample. The filters constantly clog and need to be replaced. To remedy this, a development on a filtration system aided by an electric field to help minimize filter clogging has begun. A prototype dead end filter (figure 2-6) has been built and a tangential flow filter has been designed (figure 2-7). Initial trial runs indicate that we can significantly increase filter life with this type of system.

This type of filter may also prove beneficial in separating the cryptosporidium oocysts from the waste water. The pH_{pzc} of *Cryptosporidium* has been reported to be between 2 to 3 (Brush et al., 1998, Drozd and Schwartzbrod, 1996, Karaman et al., 1999) so they would be captured on the anode. However, zeta potential

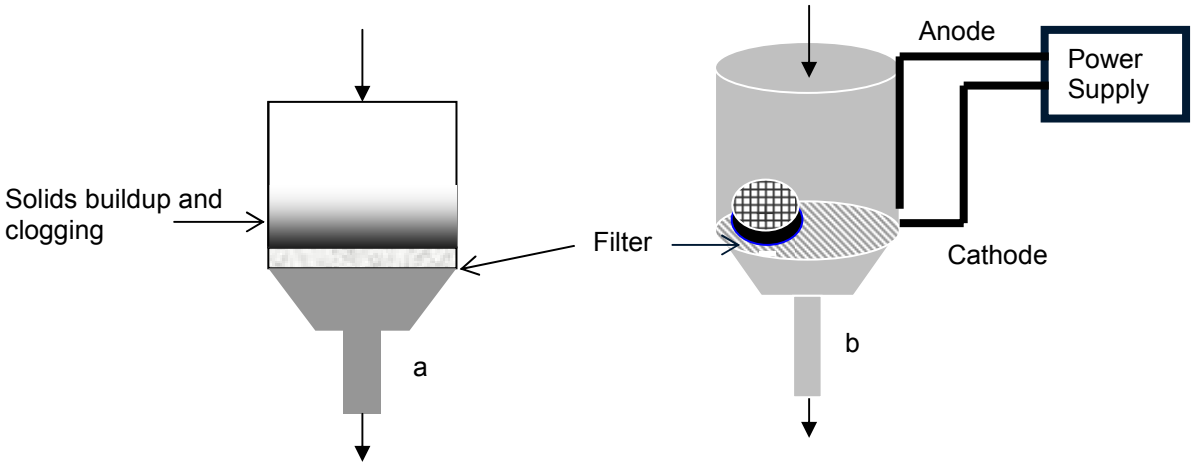

Figure 2-6 – Dead-end Filtration (a), Electric Aided Dead-end Filtration (b).

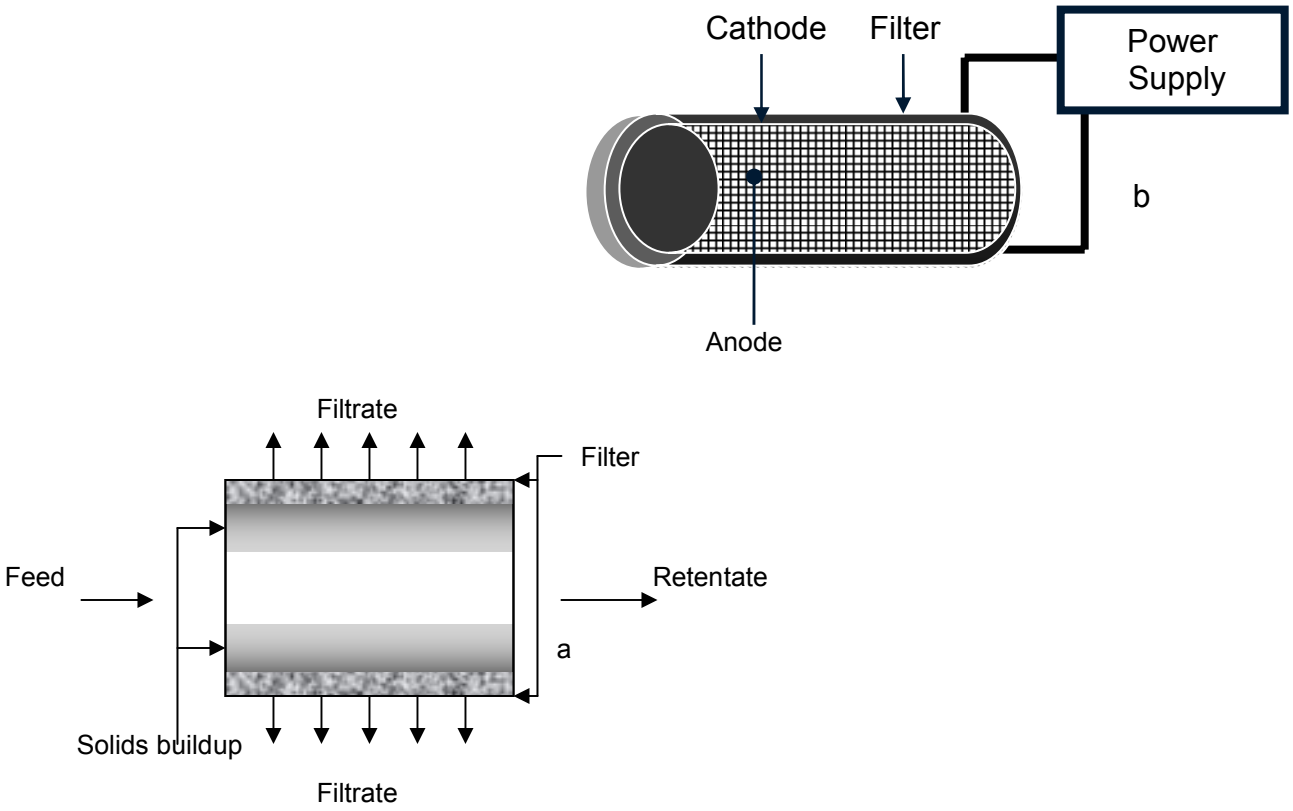

Figure 2-7 – Cross Flow Filtration (a), Electric Field Aided Cross Flow Filtration (b).

measurements that were taken when evaluating different zeta potential analyzers indicated that the pH_{pzc} was near 7 and that there was very little electrophoretic mobility. This is in agreement with reports that the surface characteristics are greatly affected by the oocyst purification method (Brush et al., 1998). The oocysts that were bought were purified using the sucrose flotation method; other methods utilize ethyl acetate that may possibly react with the oocyst surface. The potential of *Cryptosporidium parvum* oocysts and *Giardia* cysts were determined using a Malvern 3000 Zeter-meter. Figures 2-8 and 2-9 illustrate the results.

The second approach taken was to add a coagulant to the waste water. Figure 2-10 illustrates the effect on turbidity when alum is added to the waste water. A 5x10-4 M was used as the final concentration in our pretreatment of waste water samples. Figure 2-11 shows the effect of pH on the flocculation process. The addition of alum significantly reduced the turbidity of the sample. The value of the initial turbidity was measured following the same procedures as the samples treated with alum. Prior to settling, the initial turbidity of the WWTP sample was 40.3 NTU.

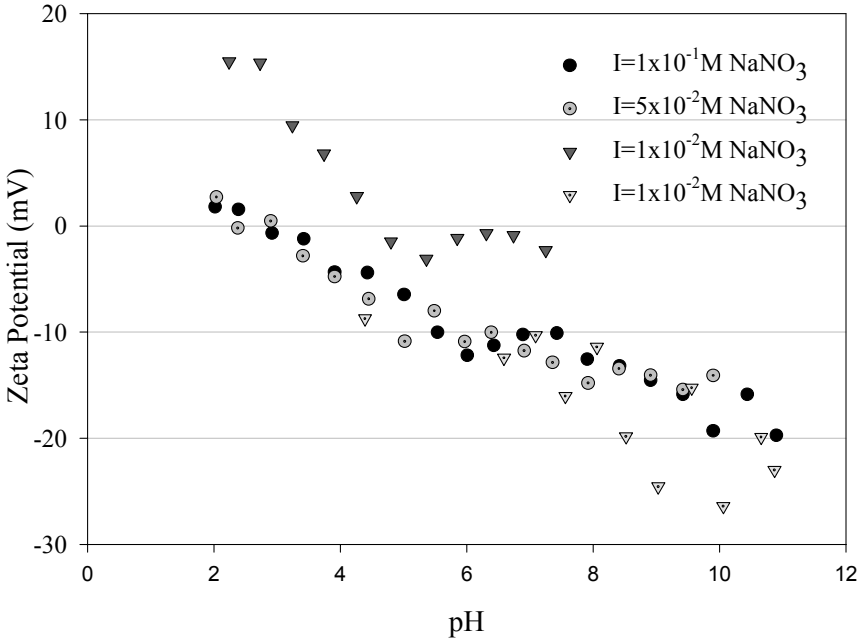

Figure 2-8 – *Giardia*; Zeta Potential Versus pH.

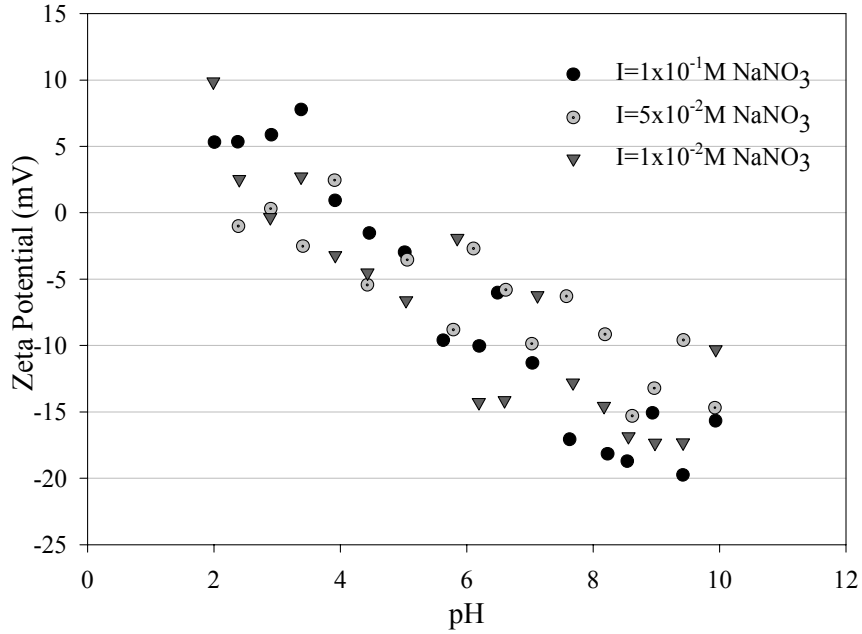

Figure 2-9 – *Cryptosporidium*; Zeta Potential Versus pH.

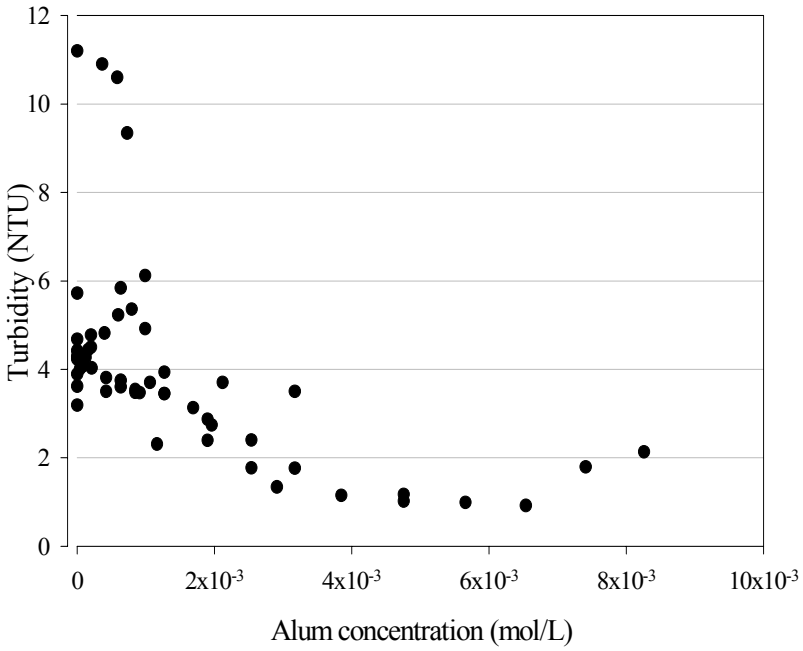

Figure 2-10 – Effect of Alum Addition on the Turbidity of WWTP Effluent.

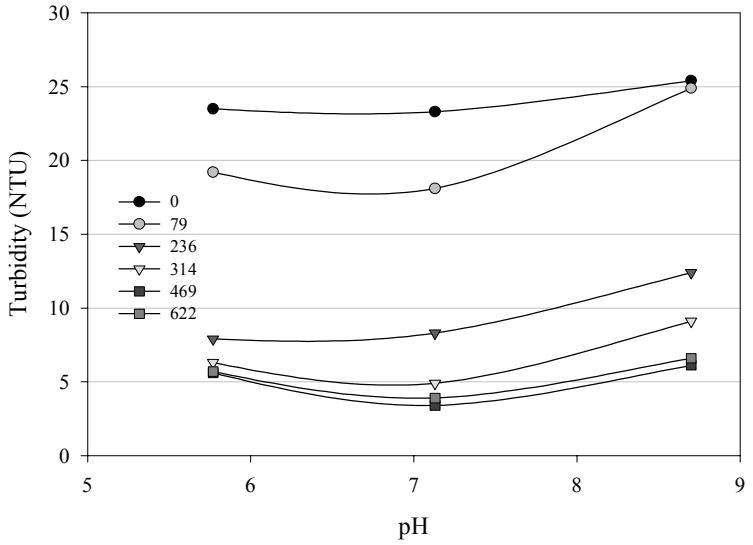

Figure 2-11 – Effect of Alum Concentration (μM) on Turbidity at Various pH Values.

2.2.3 Turbidity

The degradation of the titanium tip had an enormous effect on turbidity measurements when experiments were carried out using the probe style reactor. Use of the Nearfield™ reactor can minimize the effect of broken titanium tip on turbidity measurements. Preliminary experiments indicate that the ultrasonic treatment process does not significantly affect sample turbidity (figure 2-12).

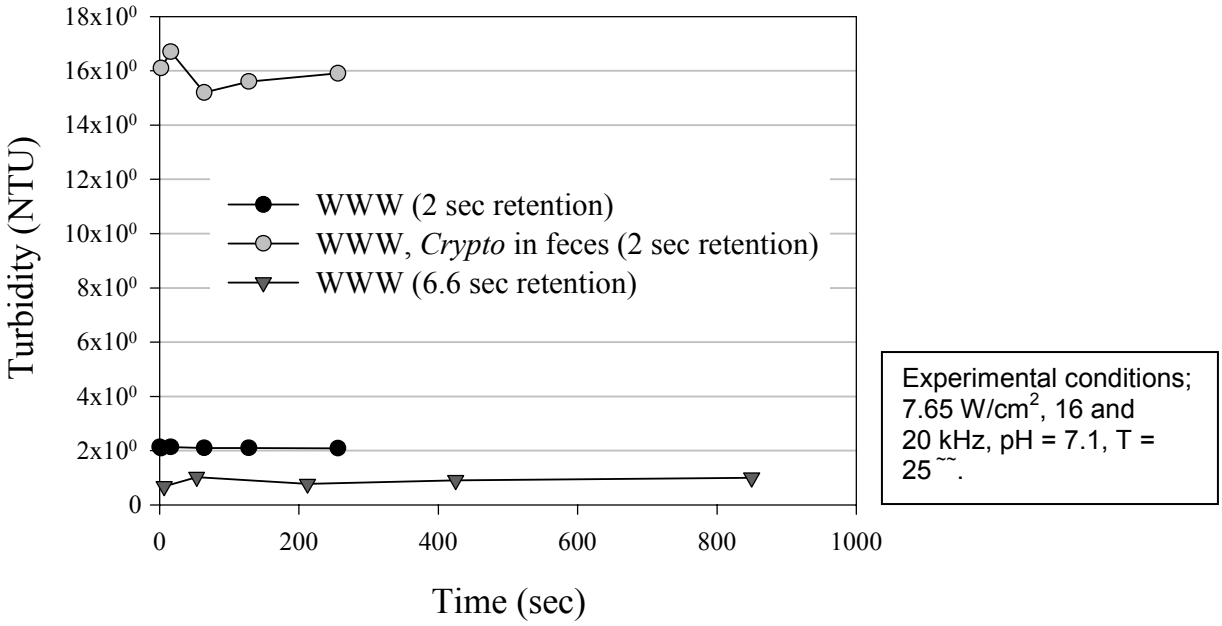

Figure 2-12 – Turbidity After Ultrasonic Treatment.

2.2.4 TOC Removal

Final effluent from the Blue Plains Waste Water Treatment plant was sonified in the batch mode using an ultrasonic intensity of 7.65 W/mL, 16 and 20 kHz, 1.59 inch reactor depth, pH 6.9, T = 25 °C. The total organic carbon (TOC) content of the waste water was determined using a Tekmar-Dohrmann DC-190 TOC analyzer (Rosemount Analytical Inc., Dohrmann Division, Cincinnati, OH). Figure 2-13 illustrates the effect of ultrasonic treatment with and without alum addition. Figure 2-14 illustrates the effect of ultrasonic treatment with alum addition on WWTP samples (batch mode).

2.2.5 BOD5 Removal

After ultrasonic treatment (7.65 W/cm^2, pH 6.9, T=25 °C, batch mode), BOD_5 measurements were carried out following the Respirometric Method 5210-D (Standard Methods, 1995) using a Bioscience BI-1000 respirometer. The oxygen uptake was continuously measured over a 5-day period. The following nutrients and organisms were added to Wilmington waste water treatment plant effluent that had been subjected to sonification (7.65 W/mL, pH 7.0, T = 25 °C, dual frequency, batch mode) for different time durations:

> To sample: 2.5 mL phosphate buffer, 0.1 mL $FeCl_3$, 0.22 mL $MgSO_4$, 0.65 mL NH_4Cl, 1.0 mL $CaCl_2$, 1.0 mL trace elements, 1.0 mL yeast, 30 mL seed (Microcat-XR, 2.0 g/L supernatant-mixed 4 hrs), 963.53 mL sample

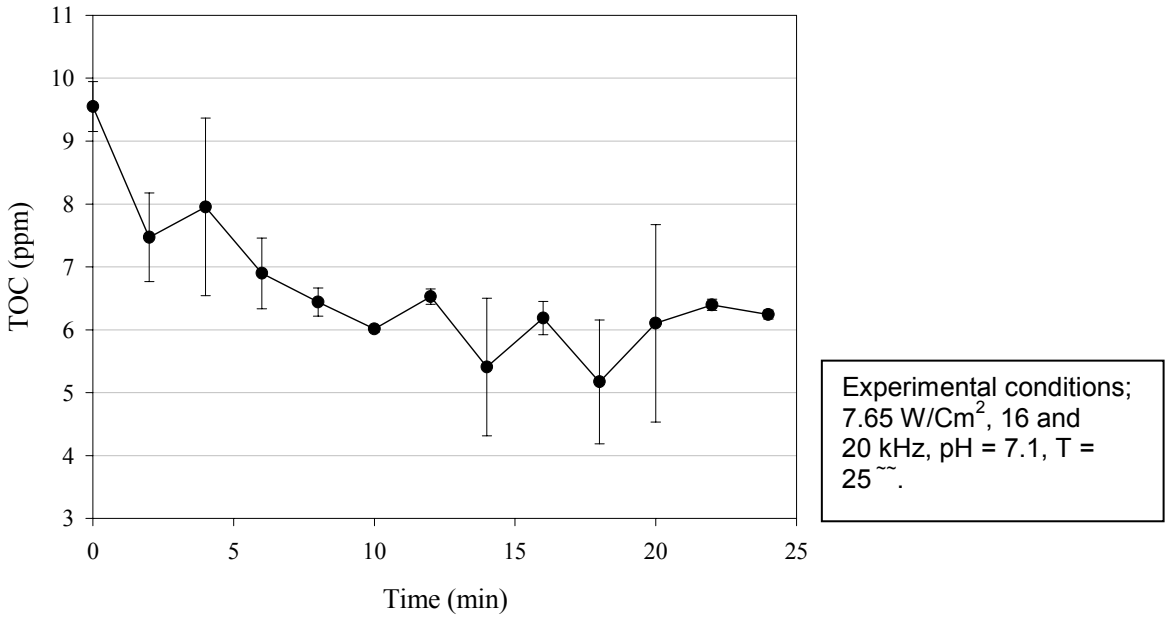

Figure 2-13 – The Effect of Alum Addition on TOC after Ultrasonic Treatment.

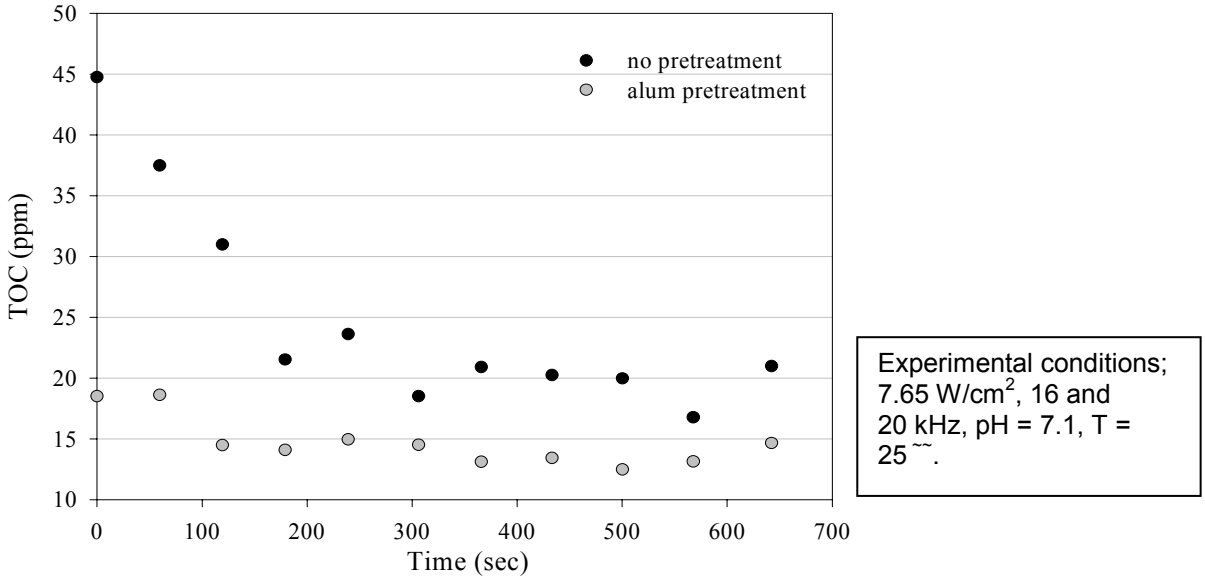

Figure 2-14 – The Effect of Ultrasound on TOC, Batch Mode.

To control: 10 glucose-glutamic acid, 6 mL phosphate buffer, 2.0 mL $FeCl_3$, 2.0 mL $MgSO_4$, 2.0 mL NH_4Cl, 2.0 mL $CaCl_2$, 2.0 mL trace elements, 30.0 mL seed, 946 mL DI H_2O

To seed blank: 10 mL glucose-glutamic acid, 6 mL phosphate buffer, 2.0 mL $FeCl_3$, 2.0 mL $MgSO_4$, 2.0 mL NH_4Cl, 2.0 mL $CaCl_2$, 2.0 mL trace elements, 500.0 mL seed, 474 mL DI H_2O

The CO_2 generated during the 5 days was captured in a NaOH trap so it would not inhibit the growth of the seed organisms. The seed blank and control blanks were run to determine the amount of BOD_5 added to the sample in the seed solution and measure endogenous decay.

Figure 2-15 illustrates the oxygen uptake over a five-day period. It reflects that the BOD_5 is increased with ultrasonic treatment. The organic constituents that are present are being degraded into forms that are more readily utilized by the bacteria. This also implies that after sonification, mineralization with other oxidizing agents will also be easier.

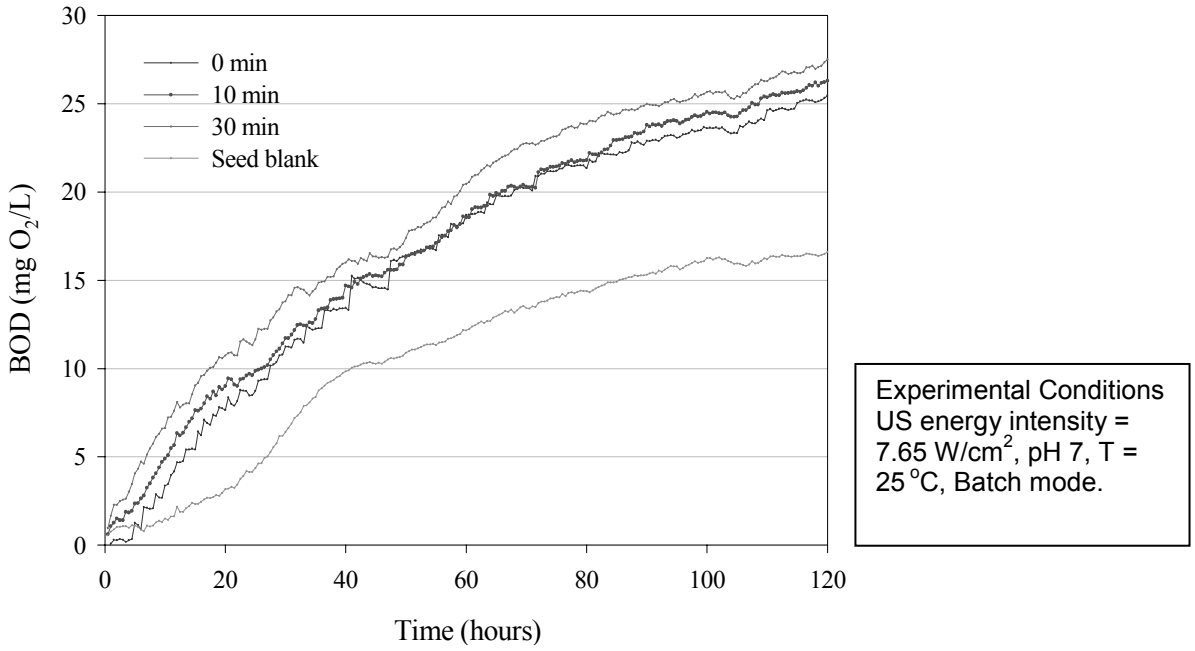

Figure 2-15 – Ultrasonic Effects on BOD_5.

2.2.6 Chemical Oxygen Demand Removal

Using the probe style reactor, accurate COD measurements were not possible due to the degradation of the ultrasonic tip. The titanium released by the tip was not consistent and the sample was contaminated in varying degrees in terms of the COD of the sample. Using the Nearfield™ reactor this phenomenon has been eliminated. Initial COD measurements indicate that there is little to no reduction in COD on raw waste water effluent samples after 20 seconds at three ultrasonic energy levels: 1,000 W, 2,000 W, 4,000 W. Figure 2-16 shows the effects of sonification on the COD of both alum treated and untreated samples and much longer time intervals. As the case with the TOC, the initial COD was less in samples that were pretreated with alum. The initial increase in COD also was less in the pretreated samples. This increase in COD, as well as THMFP, is due to the break up of larger macromolecules into smaller molecules that are easier to oxidize and more readily combine with chlorine to form DBPs.

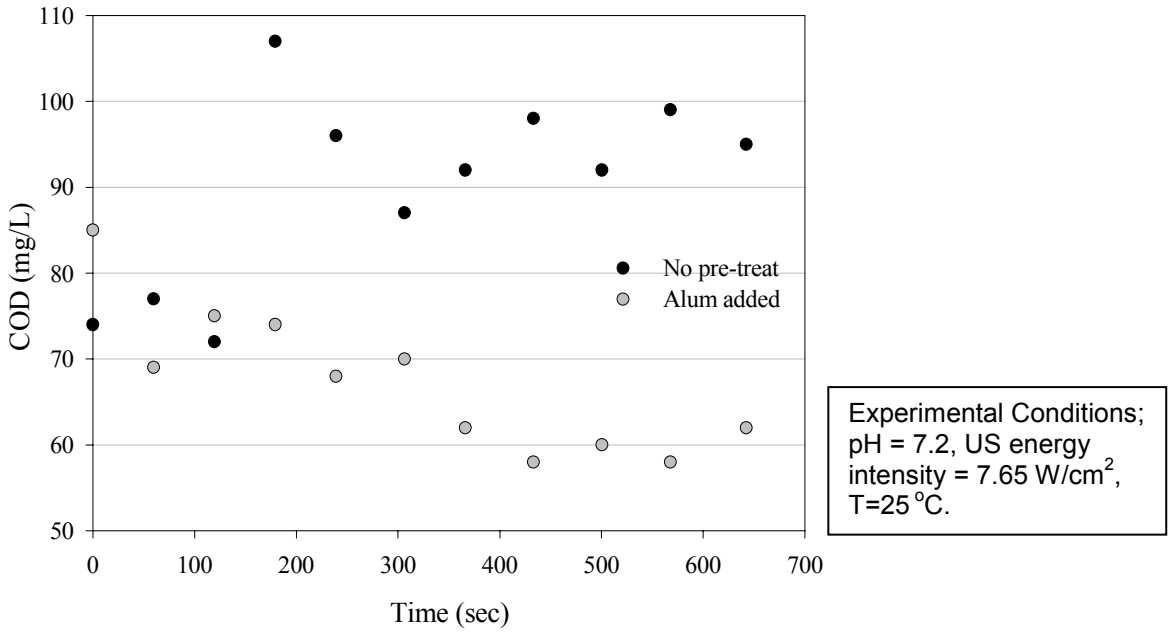

Figure 2-16 – Effect of Ultrasound on COD.

2.2.7 *E. Coli* Disinfection

Escherichia coli (E. coli) Petrifilm™ (3M) counting plates were used to determine that there were both coliforms and *E. coli* present in the WWTP effluent. The WWTP effluent samples were taken after tertiary treatment and prior to chlorination. The BPWTP and LPWTP samples were taken after chlorination and did not contain either. Both alum treated and untreated WWTP samples were sonified and the results of the untreated samples are shown in figures 2-17 and 2-18. Alum treated samples had a significantly lower initial concentration so statistically significant data was unobtainable. In the untreated samples, sonification destroyed all the coliforms and *E. coli* within 240 seconds. The

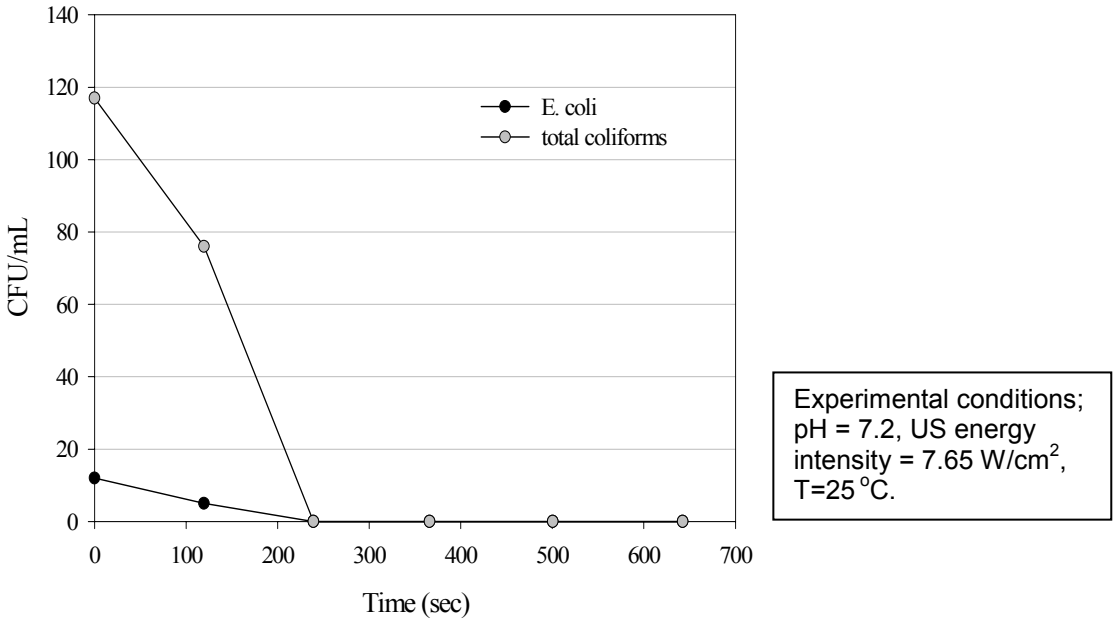

Figure 2-17 – Effect of Ultrasound on *E. coli* and Total Coliform Concentrations.

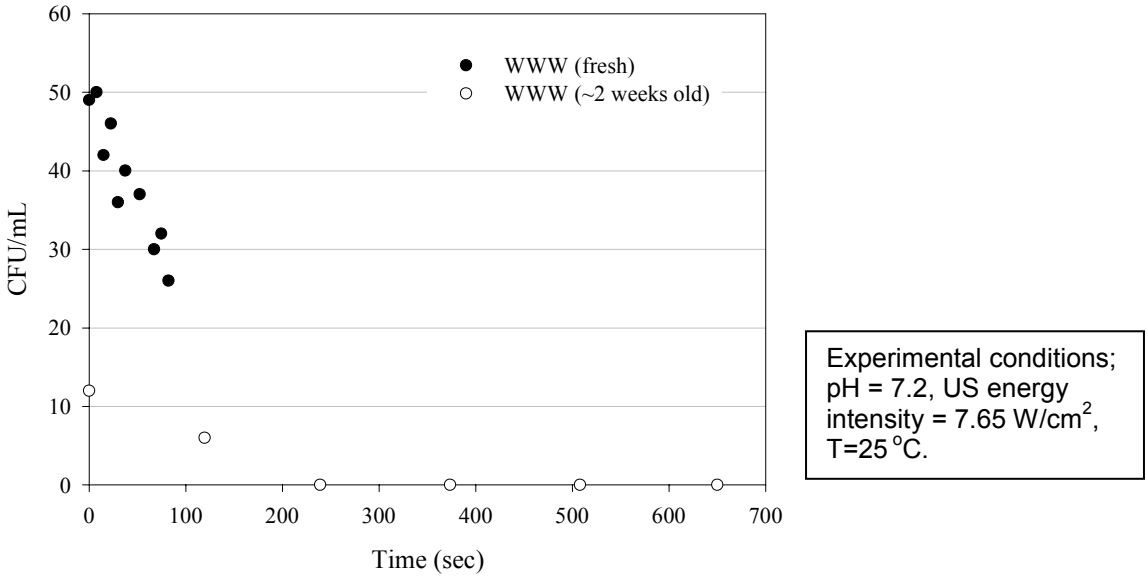

Figure 2-18 – Effect of Ultrasound on *E. coli* Concentrations.

graphs indicate that there may be an initial concentration effect. The rates of destruction of both the coliforms and the high initial *E. coli* samples appear to be greater than the lower initial concentration *E. coli* samples.

In order to prepare samples with higher and consistent bacterial levels, *E. coli* cultures were grown in the lab. Dehydrated *E. coli* culture loops were purchased from Remel labs and rehydrated in tryptic soy broth (TSB) and plated on sheeps blood agar (SBA). After an incubation period of 1 day at 37 °C, the colonies were transferred into flasks containing 300 mL of TSB and placed in a waterbath shaker, also at 37 °C. After approximately 1 day a stable concentration was reached (figure 2-19). This stock solution was used to spike the samples to be tested. After 5 days, 30 mL of the stock solution was added to 270 mL of fresh TSB to maintain a constant stock.

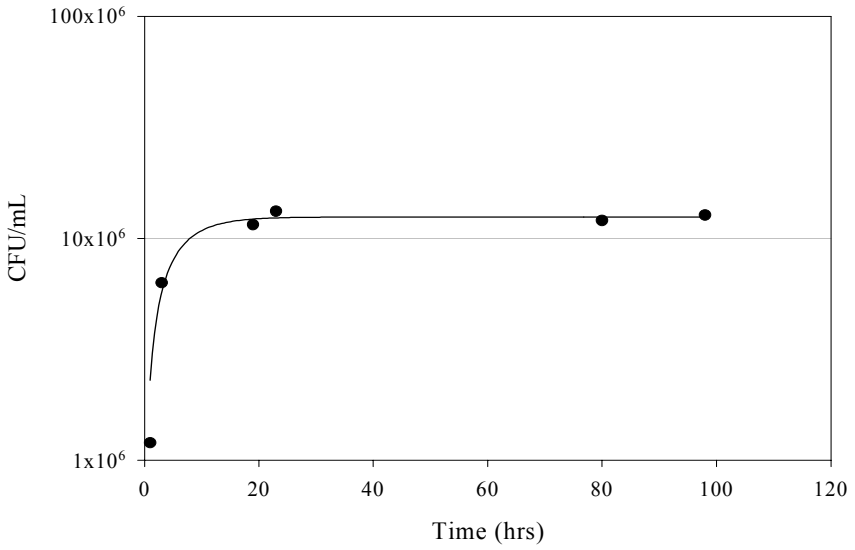

Figure 2-19 – *E. coli* Growth Curve.

Distilled water was spiked with 10 mL of stock solution and 50 mL of 150 mM Phosphate buffer solution (PBS). The final volume of the sample was 2,710 mL and the pH was 7.0. The spiked sample was then poured into the Nearfield™ processor and subjected to 2 minutes of ultrasonic treatment. The sample was drained, stirred for 5 minutes, and plated on 3M Petrifilm™ counting plates for *E. coli*. Triplicate dilutions of 10^{-4} and 10^{-5} were plated to ensure accuracy. The sample was then returned to the processor for further sonification.

The initial concentration of the spiked samples was approximately 10^6 CFU/mL, the temperature was controlled at 25 °C, the reactor depth was 1.59 inches, and the ultrasonic energy intensity was 7.65 W/cm^2 at the transducer plates. Figure 2-20 illustrates the ultrasonic destruction in the batch mode.

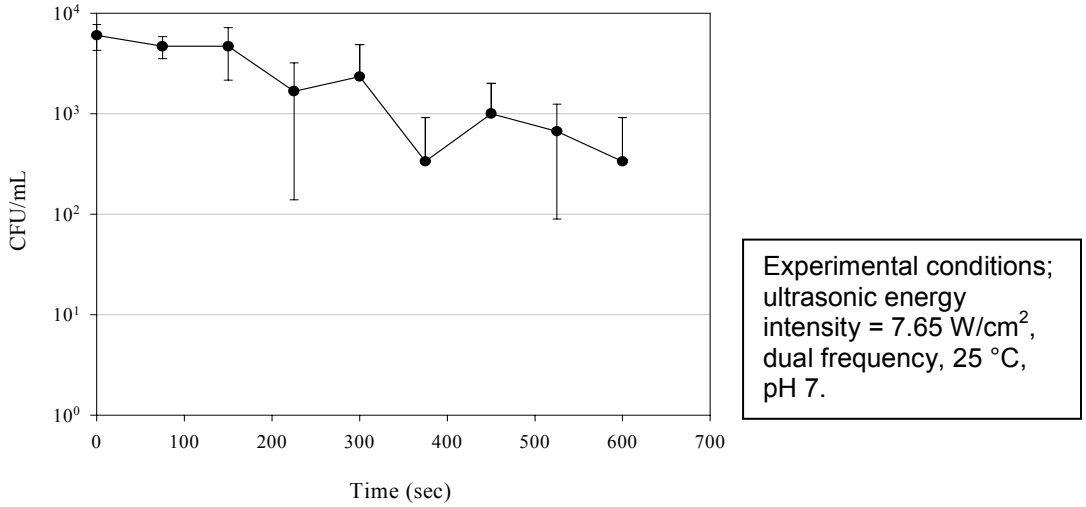

Figure 2-20 – *E. coli* Destruction, Batch Mode.

Figure 2-21 shows previous destruction curves done in the continuous recirculation mode for comparison. The continuous recirculation samples were subjected to 16 kHz or 20 kHz frequencies, the batch experiments were done using both frequencies.

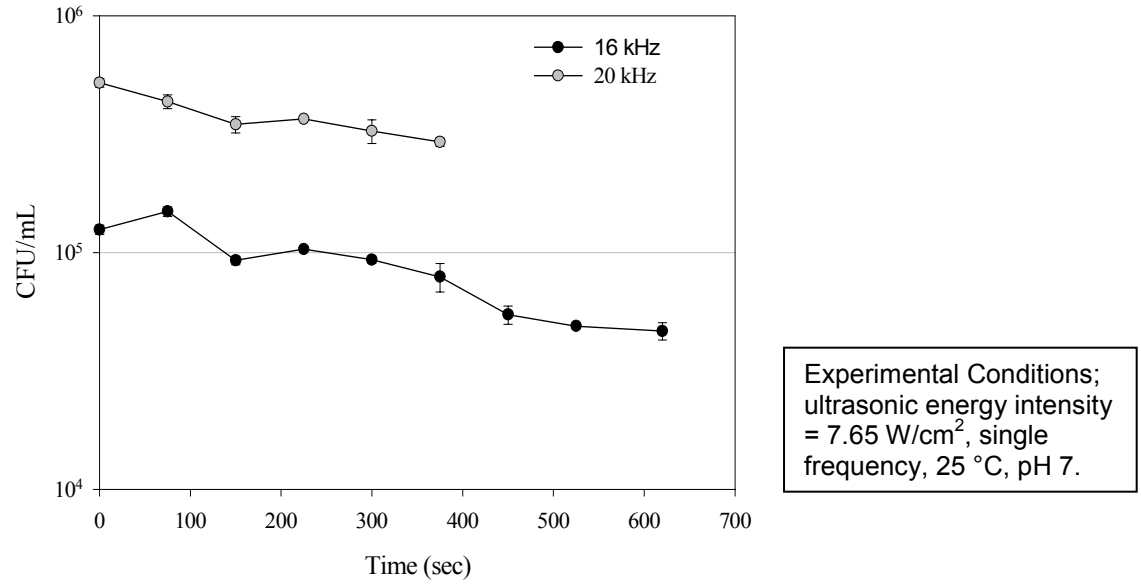

Figure 2-21 – *E. coli* Destruction with Recirculation.

2.2.8 THMFP Reduction

After sonification, 0.32 mL of chlorine dosing solution and 0.48 mL of phosphate buffering solution (pH 7.0) were added to 24 mL of sample and stored in the dark at 25 °C for 7 days. After this time period, 0.75 mL of sample was transferred into a 2-mL gas chromatograph (GC) vial and the THMs were extracted using the

liquid-liquid extraction method (0.75 mL hexane). The THM concentration was determined with a gas chromatogram (Hewlett-Packard 5890 Series II) equipped with a Vocarb 2-5320 column (L = 30 m, internal diameter = 0.53 mm, 3.0 µm film), a Hewlett-Packard model 7376 autosampler injector, and a electron capture detector (ECD). Nitrogen was the carrier gas set at a flow rate of 30 mL/min. The temperatures of the injection port and detector were 250 °C and 300 °C, respectively. The temperature program began at 50 °C and was held for 3 min., followed by a 10 °C/min ramp until a final temperature of 150 °C was reached and held for 2 min.

Figure 2-22 shows the effect of ultrasound on the THMFP. In the untreated sample the THMFP initially increased but in the alum treated sample there was no initial increase. The alum treatment decreased the initial THMFP. This indicates that many of the DBP precussors may be removed by coagulation. Figure 2-23 illustrates the GC/ECD results of a typical sample. There were two unidentified peaks that were generated.

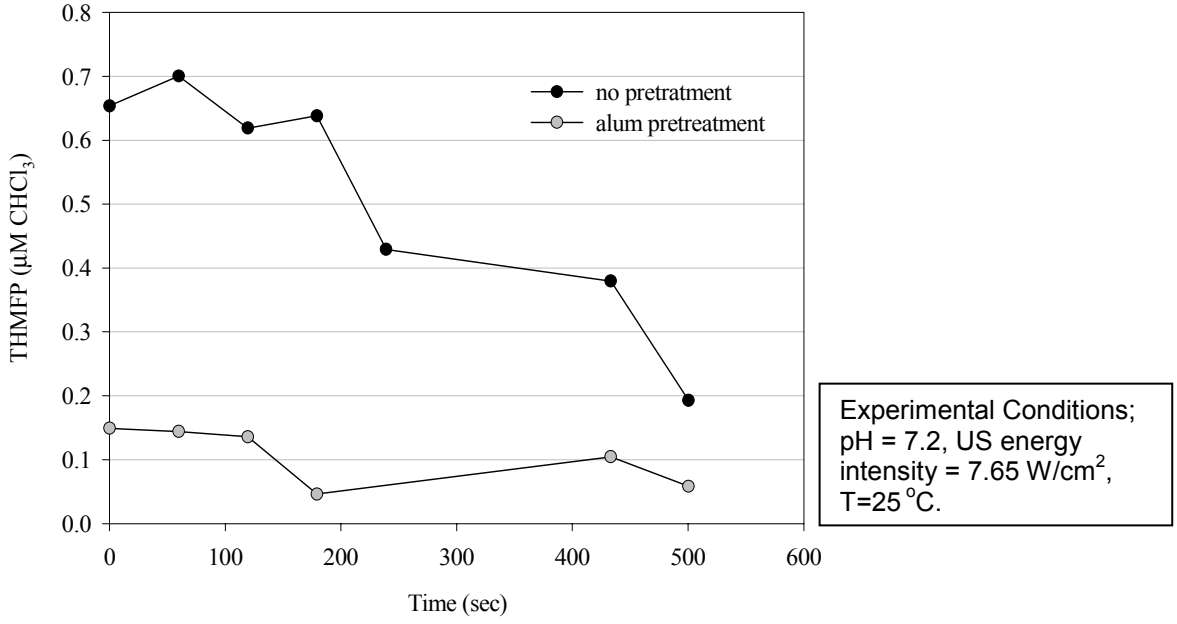

Figure 2-22 – Effect of Ultrasound on THMFP.

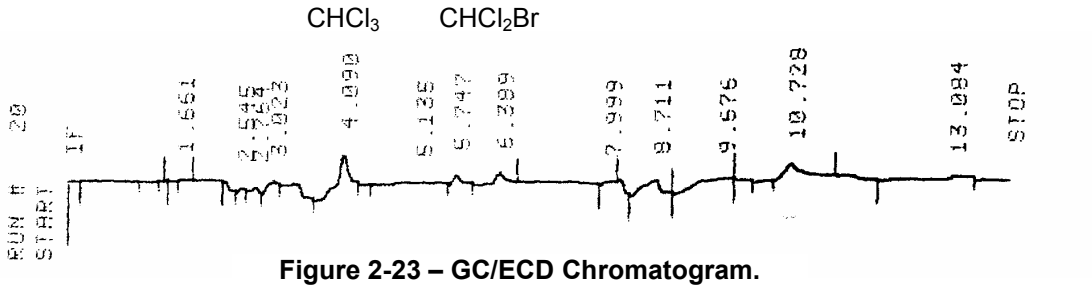

Figure 2-23 – GC/ECD Chromatogram.

GC/MS analysis was performed in an attempt to identify these unknown peaks generated during THM analysis with a gas chromatograph (Hewlett-Packard 5890 Series II) equipped with a HP 5971 mass selective detector and a HP-5MS capillary column (30 m × 0.25 mm i.d. × 0.25 μm film thickness). The injection port temperature was 300 °C and the column temperature, initially 50 °C, was held constant for 2 min, then increased to 250 °C at a ramp rate of 8 °C/min over a 30-min run time. The GC/MS interface line was maintained at 300 °C. The mass selective detector was scanned at a rate of 1.2 seconds per decade from mass 50 to 550 grams. The mass spectra were produced using the standard electron ionization (70eV) in electron impact (EI) mode. Due to the low concentrations of the contaminants, the unknowns have not been identified yet but it is suspected that they are from column bleed and/or the solvent (hexane).

2.2.9 Cryptosporidium Disinfection

Spiked waste water samples (1.75L, 10^5 oocysts/mL) were subjected to ultrasonic irradiation. Samples (38 mL) were drawn every 40 seconds and analyzed following the procedure previously outlined in earlier chapters. Figure 2-24 illustrates the results of a typical run. Results from experiments carried out with the probe reactor indicate that the reaction is first order, it seems that is the case with this reactor as well.

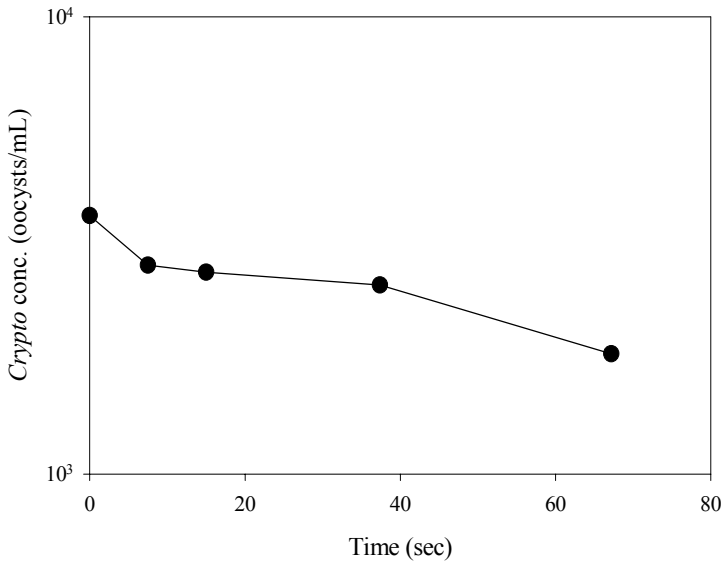

Figure 2-24 – Effect of Ultrasound on *Cryptosporidium* Concentration, Experimental Conditions; pH = 7.2, US energy intensity = 7.65W/cm^2, T = 25 °C

2.3 Retention Time Calculation

2.3.1 Plug Flow

Retention time calculation proved to be more difficult than initially anticipated. The reactor was designed to continuously recycle the sample because sample

volume was limited. The retention times given up until this point were calculated based on a plug flow reactor model. The following is a model of the retention time calculation that was initially used:

V_T = initial volume (L)
V_S = volume sampled = t_S*Q (L)
V_c= sum of volume in reactor and CSTR
=V_R+V_B (L)
Q = flow rate (L/sec)
t_T = total time (sec)
t_R = time in reactor = V_R/Q (sec)
t_L = time in loop = (V_T-L*V_S)/Q (sec)
V_B = volume of CSTR = V_T – L*V_S-1.06 (L)

$$L = \sum \frac{t_{Tt,i} - t_{Tt,i-1}}{t_{L,i}} = \#\text{ of loops}$$

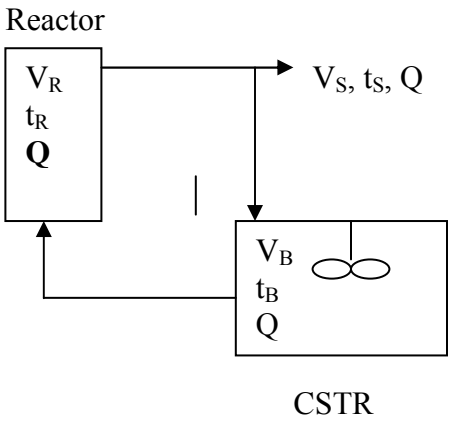

Total Retention Time = L*t_R

The assumption that the recirculation rate is high enough so that the conversion per pass is low was made so that the system could be modeled as a batch reactor. V_T and V_S are minimized, the reaction is first order, and complete and instantaneous mixing in the CSTR are assumed. Modeled as a batch reactor the governing equation is:

$$t = \sum_{i=0}^{n} \frac{V_{B,i}}{V_R} \int_{C_{AF}}^{C_{A0}} \frac{dC_A}{-r_A} \qquad (5.1)$$

where r_a is the reaction rate.

2.3.2 Tracer Tests

To verify the assumption that there is instantaneous and complete mixing in the CSTR, NO_3^{2-} was spiked into the CSTR and measured at the sampling port immediately after the pump. Periodically, 25-mL samples were drawn and 0.5 mL 1N HCl was added. NO_3^{2-} analyses were performed on these samples with a Hewlett Packard Spectrophotometer measuring 220 nm absorbency in a quartz cell (1 cm path length). Figures 2-25 and 2-26 illustrate the results of the tracer tests. Total mixing within the CSTR was achieved in less than 5 seconds so it was determined that the assumption would be valid.

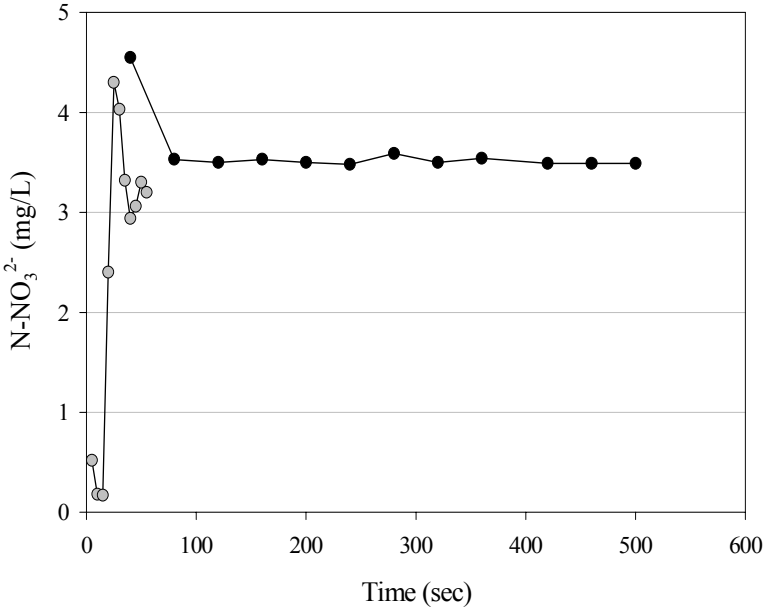

Figure 2-25 – Tracer test, $N\text{-}NO_3^{2-}$ Concentration at the Sampling Port.

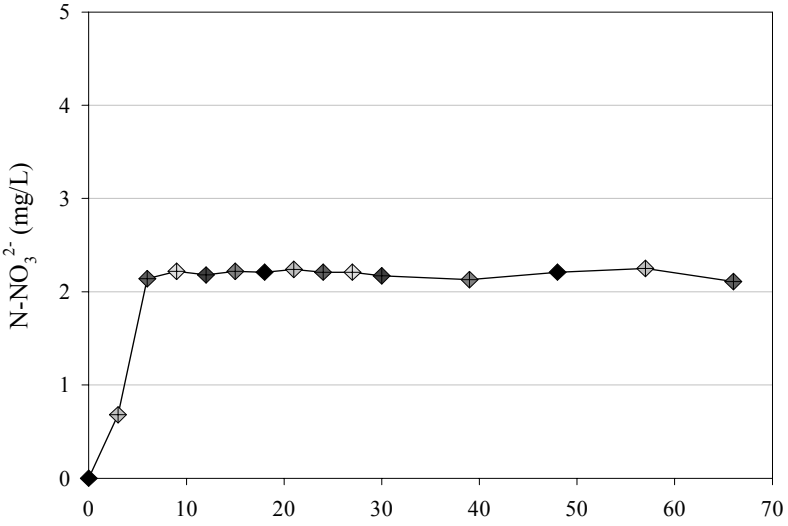

Figure 2-26 – Tracer Test. Nitrate Concentration at Point Right After the Pump.

2.3.3 Dispersion Model

A dispersion model was developed to model the flow pattern in the Nearfield™ acoustical processor when it was running in the continuous recirculation mode. Modeling was accomplished by incorporating a recirculation component in a model reported by Levenspeil (1972). The dispersed plug flow model

(figure 2-27) was used to illustrate the flow within the reactor. Consider a steady flow reactor of length L through which fluid is flowing with a constant velocity, u, and in which material is mixing axially with a dispersion coefficient, D. Let the n^{th}-order reaction be of the type:

$$\text{A} \rightarrow \text{products}, \quad -r_A = kC_A^{\,n} \tag{5.2}$$

By referring to the elementary section of the reactor as shown in figure 2-27, the basic material balance for any reaction component is:

$$\text{input} = \text{output} + \text{disappearance by reaction} + \text{accumulation} \tag{5.3}$$

For component A, equation 5.3 becomes:

$$(\text{out-in})_{\text{bulk flow}} + (\text{out-in})_{\text{axial dispersion}} + \text{disappearance by reaction} + \text{accumulation} = 0$$

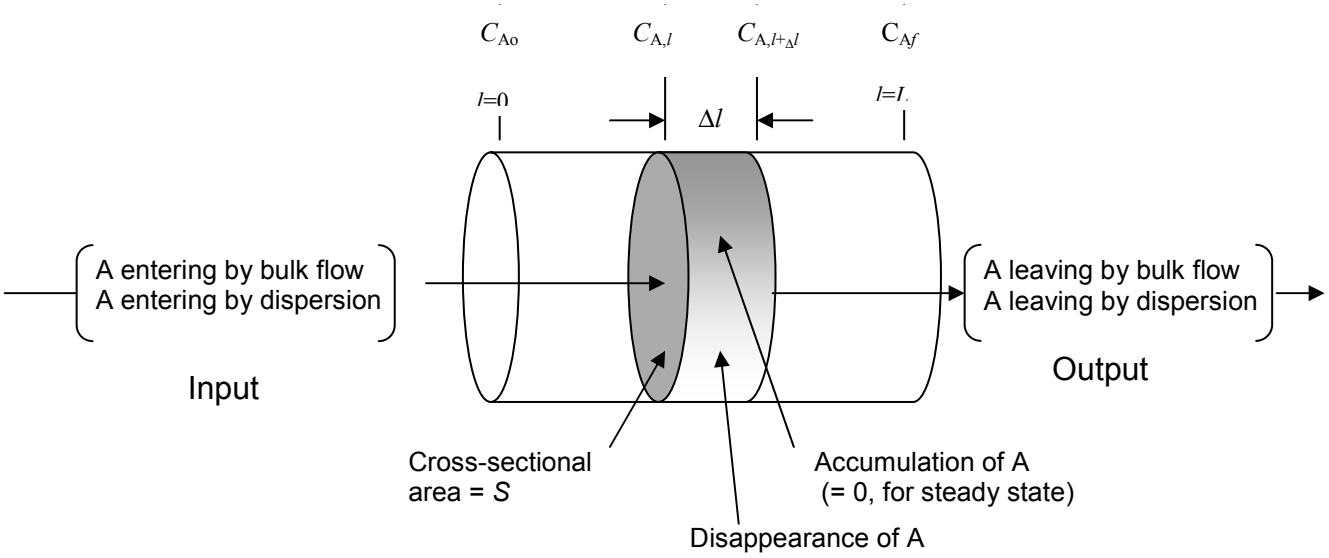

Figure 2-27 – Variables for a Closed Vessel in Which Reaction and Dispersion Are Occurring.

The individual terms (in moles A/time) are as follows:

$$\text{entering by bulk flow} = \left(\frac{\text{moles A}}{\text{volume}}\right)(\text{volumetric flow rate})$$

$$= \left(\frac{\text{moles A}}{\text{volume}}\right)(\text{cross - sectional area})(\text{flow velocity})$$

$$= (C_{A,l})Su$$

$$\text{leaving by bulk flow} = (C_{A,l+\Delta l})Su$$

$$\text{entering by axial dispersion} = \frac{dN_A}{dt} = -\left(DS\frac{dC_A}{dl}\right)_l$$

$$\text{leaving by axial dispersion} = \frac{dN_A}{dt} = -\left(DS\frac{dC_A}{dl}\right)_{l+\Delta l}$$

$$\text{disappearance by reaction} = (-r_A)V = (-r_A)S\Delta l$$

Entering all these terms into the initial equation 5.3 and dividing by $S\Delta l$ gives:

$$u\frac{(C_{A,l+\Delta l} - C_{A,l})}{\Delta l} - D\frac{\left[\left(\frac{dC_A}{dl}\right)_{l+\Delta l} - \left(\frac{dC_A}{dl}\right)_l\right]}{\Delta l} + (-r_A) = 0 \qquad (5.4)$$

Using the basic limiting process of calculus that for any quantity Q which is a smooth continuous function of l:

$$\lim_{l_2 \to l_1} \frac{Q_2 - Q_1}{l_2 - l_1} = \lim_{l \to 0} \frac{\Delta Q}{\Delta l} = \frac{dQ}{dl} \qquad (5.5)$$

Taking the limits as $\Delta l \to 0$ we obtain

$$u\frac{dC_A}{dl} - D\frac{d^2C_A}{dl^2} + kC_An = 0 \qquad (5.6)$$

In dimensionless form where $z = l/L$ and $\tau = \bar{t} = L/u = V/v$, expression 6 becomes:

$$\frac{D}{uL}\frac{d^2C_A}{dz^2} - \frac{dC_A}{dz} - k\tau C_A{}^n = 0 \qquad (5.7)$$

or in terms of fractional conversion

$$\frac{D}{uL}\frac{d^2X_A}{dz^2} - \frac{dX_A}{dz} + k\tau C_{A0}^{n-1}(1 - x_A)^n = 0 \qquad (5.8)$$

This expression shows that the fractional conversion of reactant A in its passage through the reactor is governed by three dimensionless groups: a reaction rate group, the $k\tau C_{A0}^{n-1}$ dispersion group D/uL, and the reaction order n. Wehner and Wilhelm (1956) solved this equation analytically for first-order reactions; the solution is:

$$\frac{C_A}{C_{A0}} = 1 - X_A = \frac{4a\exp\left(\frac{1}{2}\frac{uL}{D}\right)}{(1+a)^2\exp\left(\frac{a}{2}\frac{uL}{D}\right) - (1-a)^2\exp\left(-\frac{a}{2}\frac{uL}{D}\right)} \qquad (5.9)$$

where $a = \sqrt{1 + 4k\tau(D/uL)}$

Figure 2-28 represents the reactor setup with continuous sample recirculation.

V_T = initial volume (L)
V_S = sample volume (L)
V_R= reactor volume (L)
V_C= CSTR volume (L)
C_R = Concentration in reactor (#/mL)
C_C = Concentration CSTR (#/mL)
Q = flow rate (L/sec)
$t_R = V_R/Q$ (sec)
$t_C = V_B/Q$ (sec)
n = # of complete cycles

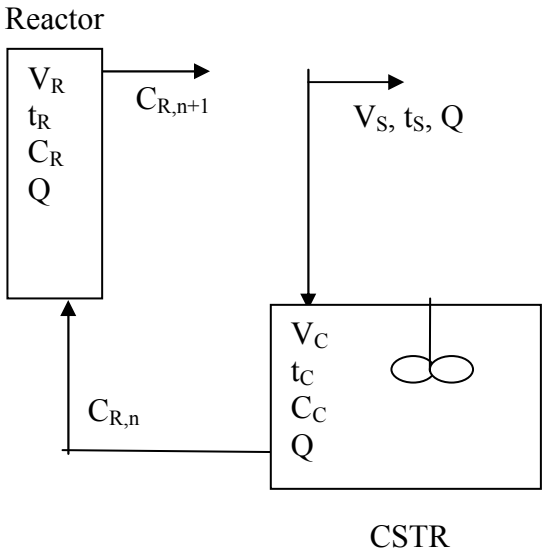

Figure 2-28 – Schematic Diagram of the Flow Pattern with Recirculation.

Dilution of the sample in the CSTR due to the recirculation is expressed as follows:

$$C_C = \frac{2C_{R,n}V_C - C_{R,n}V_R + C_{R,n+1}V_R}{2} \text{ for all } n \geq 1 \qquad (5.10)$$
$$C_C = C_{R,n} \text{ for all } n = 0$$

Incorporating the dilution term (equation 10) into equation 9, we arrive at the final solution:

$$C_{R,n+2} = \left(\frac{2C_{R,n}V_C - C_{R,n}V_R + C_{R,n+1}V_R}{2} \right) \left(\frac{4a \exp\left(\frac{1}{2} \frac{uL}{D} \right)}{(1+a)^2 \exp\left(\frac{a}{2} \frac{uL}{D} \right) - (1-a)^2 \exp\left(-\frac{a}{2} \frac{uL}{D} \right)} \right) \text{ for n} \geq 1$$

$$C_{R,n+1} = C_{R,n} \left(\frac{4a \exp\left(\frac{1}{2} \frac{uL}{D} \right)}{(1+a)^2 \exp\left(\frac{a}{2} \frac{uL}{D} \right) - (1-a)^2 \exp\left(-\frac{a}{2} \frac{uL}{D} \right)} \right) \text{ for all n} = 0 \qquad (5.11)$$

Equation 5.9 (no recirculation) and 5.11 (with recirculation) can be used to model the ultrasonic system. The concentrations can be measured, D can be calculated based on tracer tests, and the reactor dimensions and flow rate are known, leaving *k* as the only unknown variable. Figure 2-29 illustrates model predictions (equation 5.11) against experimental data for a system with the following characteristics:

u = 1.084 cm/sec
L = 68.58 cm
D = 70,000
τ = 63.27 sec
uL/D = 1.06 x 10^{-3} cm^2/sec

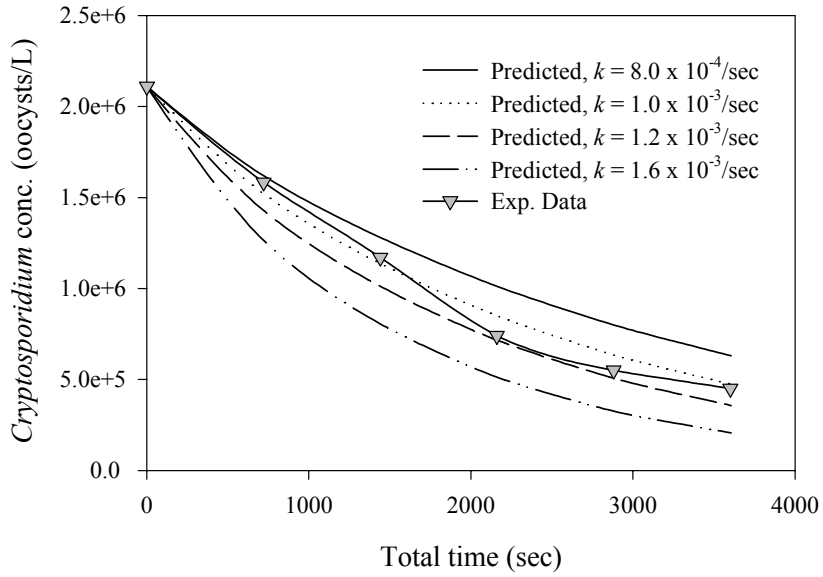

Figure 2-29 – Model Prediction Versus Experimental Data.

Waste water effluent was treated in the tri-frequency ultrasonic system (Chapter 6, exp. cond.: 2,000 W 16 kHz, 2,000 W 20 kHz, 360 W 1.7, Hz, 21 μM H_2O_2/sec, pH = 7, T = 25 °C, flow rate = 1.7 L/min, sample vol. = 4 L , reactor vol. = 1.7 L, spacer width = 1¼"). The experimental data and model prediction are excellent and the k value under these conditions is ~ 1.1 x 10^{-3}/sec.

2.3.4 Ultrasonic Wave Modeling

Modeling the wave pattern in the reactor was considered but it was concluded that time and technical limitations would not permit development of an accurate model. The reaction chamber is enclosed so there is no way to determine the actual wave profiles without cutting out portions of the transducer plates and inserting receivers. Without this information it is impossible to describe what is happening within the reactor. Factors effecting the waves include: initial frequency and intensity, reflection off opposing walls, superposition, wave speed (traveling through liquid and air – cavitation bubbles), transducer plates bolted onto each other, and temperature. The amplitude of the sound wave will be assumed to be based on the equations of superposition, that is:

$$y = \left(2y_0 \cos 2\pi \left(\frac{f_1 - f_2}{2} \right) t \right) \sin 2t \left(\frac{f_1 - f_2}{2} \right) t \qquad (5.12)$$

where: f = frequency
t = time

Wave intensity within the reactor is calculated using the equation:

$$I_1 4\pi r_1^2 = I 24\pi r_2^2 \qquad (5.13)$$

where: r = distance from transducer
I = intensity (W/cm^2)

2.4 Summary

The effect of the addition of $Al_2(SO_4)_3 \bullet 13\ H_2O$ (alum) as a pretreatment was investigated and found to be beneficial with respect to the reduction of total organic carbon (TOC), trihalomethane formation potential (THMFP), chemical oxygen demand (COD), *E. coli* concentration, and turbidity. The coagulation and flocculation step is normally carried out during water treatment so it doesn't represent any additional costs in terms of the final goal of waste water reclamation. As an alternative to the coagulation process, a filtration system aided by an electric field was designed and a prototype was built. We hope that this type of filtration system will help reduce disinfection by-product (DBP)

precursors as well as aid in decreasing the *Cryptosporidium* oocyst concentration. Currently the filtration system is being tested by another graduate student in pursuit of his doctorate.

The ultrasonic process significantly reduced the TOC. This indicates that complete mineralization of organic components was occurring. DBP precursors and other constituents that make up the organic portion of the waste water were oxidized and the overall reduction of these components was about 33 percent in 24 minutes. This time frame is still too long to be economically feasible but with the addition of H_2O_2 and/or the addition of a high frequency transducer(s) it is believed that the OH• concentration can be significantly reduced and the reaction time substantially decreased.

It is clear that the combined frequencies provide a substantial increase in destructive capacity. In 375 seconds, the destruction for the individual frequencies was between 34–43 percent while the destruction with the dual frequencies was ~99 percent. However, cost comparisons must be done to evaluate overall efficiency.

3. The Tri-Frequency Nearfield™ Acoustical Processor

3.1 Introduction

The Nearfield™ Acoustical Processor is equipped with two transducers that are facing each other (detailed schematics and photos have been provided in Appendix E). Each transducer has a unique frequency (16 kHz, 20 kHz) so we can take advantage of the pressure amplification due to the additive nature of the sound waves (superposition). This reactor has proved to be substantially more energy efficent and powerful than the probe style. However, it did not generate results that were considered satisfactory in terms of treatment time length and financial feasibility. The THMFP reduction takes place over a time frame much greater than the disinfection time frame. The financial feasibility of the organic constituent mineralization may never be achieved but it may be achieved with respect to disinfection. In an attempt to further enhance the ultrasonic process, we have designed a new spacer equipped with 17, 1.7 mHz transducers. Figure 3-1 illustrates the new reactor layout.

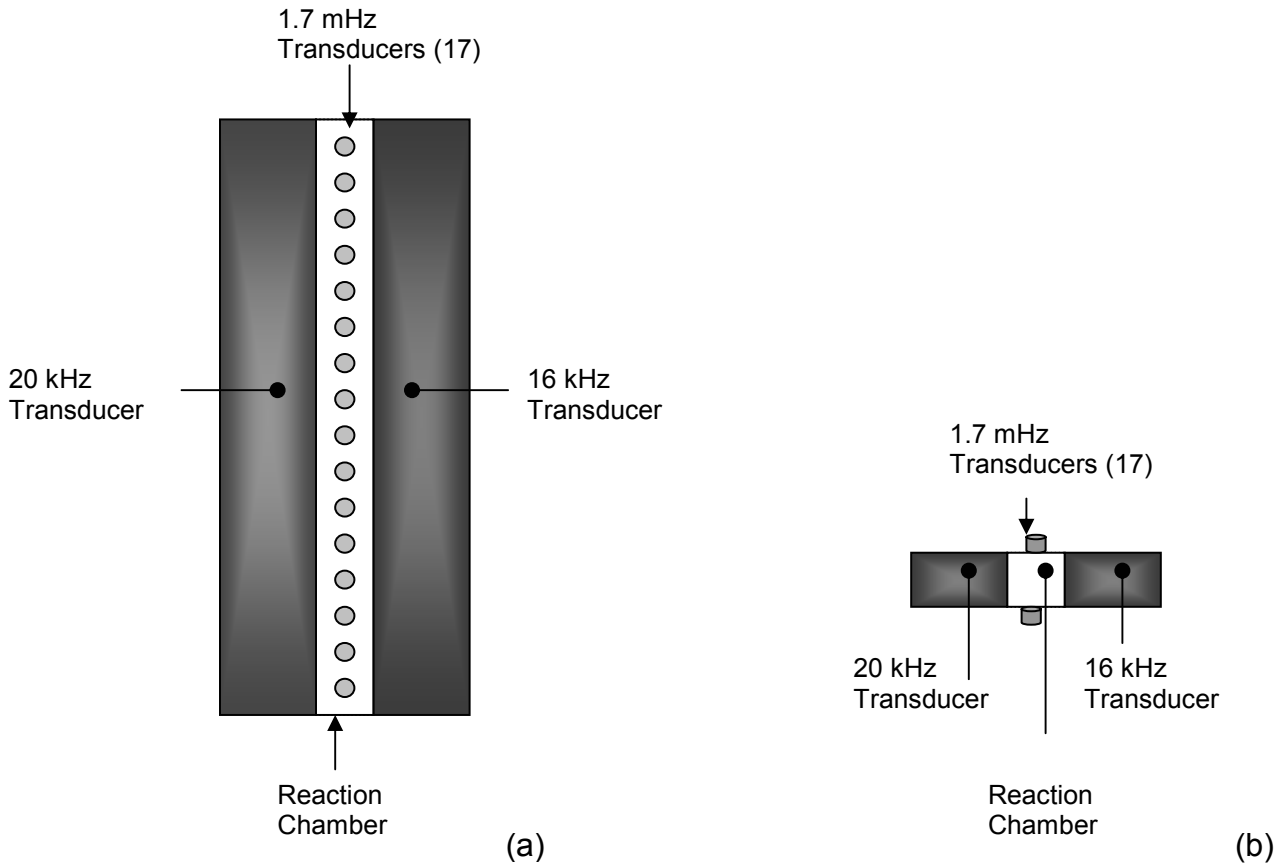

Figure 3-1 – Three Transducer Reactor Set-up: (a) Side View; (b) Top View.

The transducers are normal to the existing 16 kHz and 20 kHz transducers, creating a new, three-dimensional wave by adding the amplitudes of each wave. Although the current wave (two transducers) is also three-dimensional, the wave profile in the z direction is now constant. This will not be the case with the new system.

The superposition created when the waves are combined will create a greater amplitude magnification than that of the two transducer set up. In addition, adding the high frequency transducer should greatly enhance the OH• formation. Entezari and Kruus (1996) have shown that at higher frequencies the OH• formation is significantly increased. Their results indicated that the degredation of phenol was six times higher at 487 kHz than at 20 kHz.

Hua and Hoffmann (1997) have also reported the same phenomenon. Table 3-1 and figure 3-2 are drawn from their work and reflect the properties of the cavitation bubble and the H_2O_2 and OH• rate constants.

Table 3-1 – Compression Half-cycle Length, Bubble Collapse Time, and Resonant Bubble Radii for Ar and Kr as Saturating Gases (Hua and Hoffmann, 1997)

Frequency (kHz)	Half-cycle length (μs)	Collapse time (μs)	Resonant radius (μm)	Surface area (μm^2)	Volume (nL)
20.2	25.0	16.20	178	3.96×10^5	23.4
39.4	12.5	8.10	88.8	9.91×10^4	2.930
80.6	6.8	4.10	44.4	2.48×10^4	0.366
513	1.0	0.65	7.1	6.34×10^2	0.0015

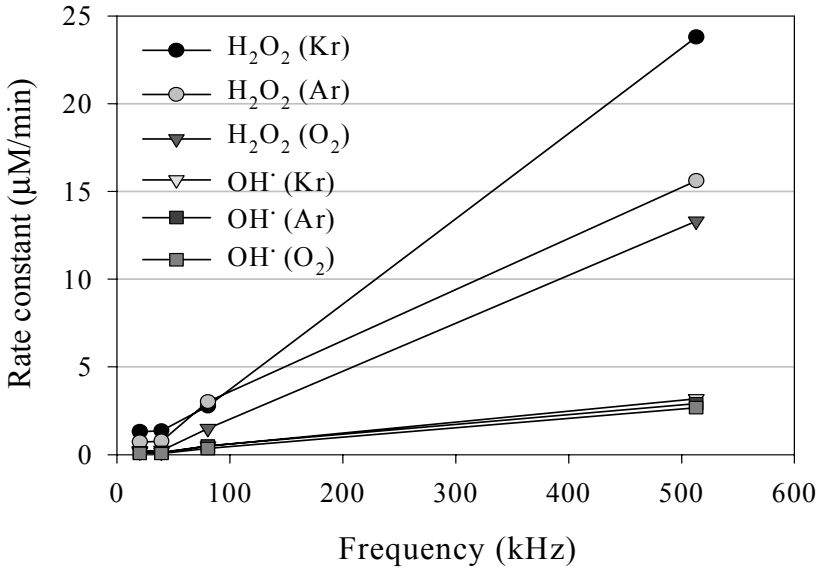

Figure 3-2 – Rate Constants for H_2O_2 and OH• Production at Various Frequencies and Saturating Gases (Hua and Hoffmann, 1997).

It is hypothesized that at lower frequencies physical destruction plays a much larger role in the degradation capacities of the ultrasonic process. The volume of the cavitation bubbles is much greater so that larger particles can be trapped within and be in contact with the exterior of the bubble. The intense heat and pressure generated during the bubble collapse would then destroy these particles, i.e. *Cryptosporidium*. The cavitation bubbles are much smaller and less stable at high frequencies. This leads to the increased production of OH•. An increase in the OH• production should greatly enhance the oxidation potential of the ultrasonic process. Figure 3-3 illustrates a close up of the transducer and the spacer with embedded transducers designed to give higher OH• concentrations.

Individual transducer

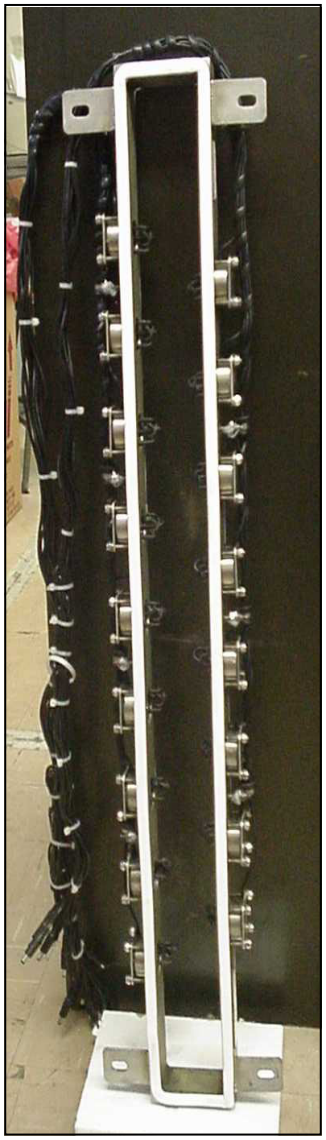

Spacer with 17 transducers

Figure 3-3 – 1.7-mHz Transducer and Spacer with Embedded Transducers.

The first tri-frequency spacer did not work and there were many problems with it. The wires on the inside of the spacer disrupted the flow. The 2" width and the energy dissipation were too great, and it leaked. TOC and COD reduction experiments revealed that there was virtually no mineralization occurring. The spacer was returned to the manufacturer and redesigned. Figure 3-4 illustrates the final version. It is 1¼" wide, the wires are on the outside, and it does not leak. The crystal transducer was separated from the original housing and the RF was placed in a water bath to keep it from overheating. This cooling configuration also gives the reactor the capability to be run in the batch mode. The RF cooling housing was isolated and uses a floating ground so that the 17 1.7-mHz transducers do not synchronize themselves. There is no return wire from the crystals, the ground travels down a neighboring crystal wire between cycles. The wiring configuration was critical so no feedback was generated that reduced the overall output of the system. The 17 transducers generated approximately 360 W and drew 19 amps. Ground fault protected power sources could not be used.

Figure 3-4 – Final Version of 1.7-mHz Transducer.

3.2 Results and Discussion

Experiments were carried out based on the previously reported methodology to test the tri-frequency design and the effect of different spacer widths. The final version of the tri-frequency spacer solved the leaking, flow inhibition, and width problems that plagued the prototype.

3.2.1 *E. Coli* Disinfection

Figure 3-5 represents the effect of the spacer width on the disinfection of *E. coli*. It is clear that the smaller the width, the greater the destructive force becomes. The trade off is the diminished sample throughput. The time it takes to achieve

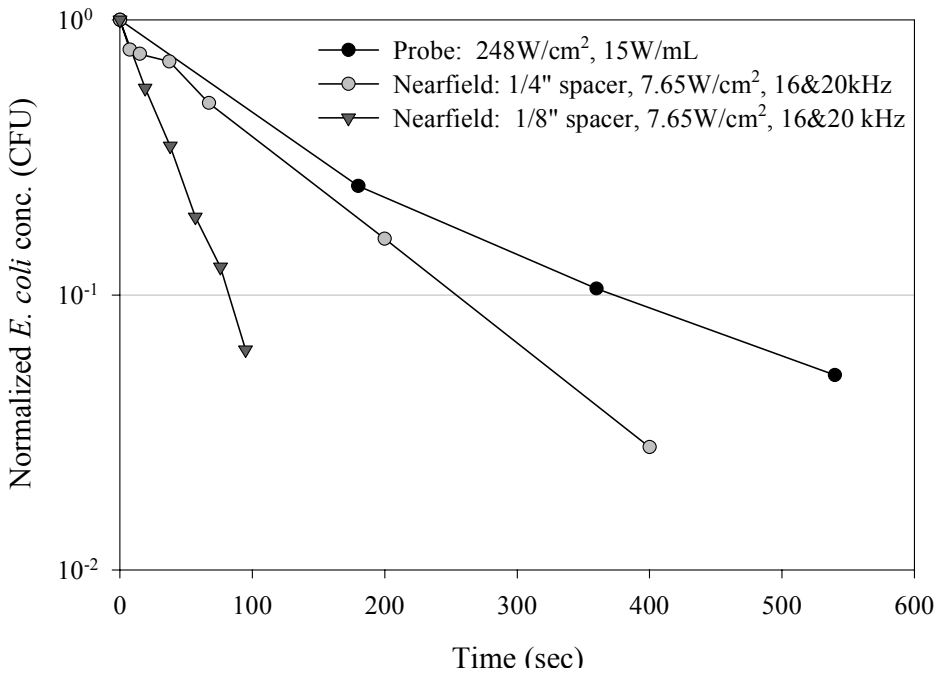

Figure 3-5 – Effect of Reactor Type and Spacer Width on *E. coli* Disinfection , Nearfield Versus Probe.

1 log removal is decreased by approximately 400 percent when comparing the probe style reactor to one with a 1/8" spacer (16 and 20 kHz).

Figures 3-6 and 3-8 illustrate the effect of the combination of frequencies and the initial concentration on the destruction of *E. coli*. The combination of 16 and 20 kHz works better than 16 or 20 kHz independently but the difference may not justify the doubling of the power expenditure.

Comparing the 1/8" spacer to the tri-spacer (1¼") with H_2O_2 is illustrated by figure 3-7. The H_2O_2 was continuously fed into the reactor just after the mixing and recirculation flask. H_2O_2 was added in an effort to improve the OH concentration above and beyond the amount generated by the addition of the high frequency reactor. The 1/8" spacer performed better than both the H_2O_2 only, and the H_2O_2 – tri-frequency combination.

3.2.2 Cryptosporidium Disinfection

Figure 3-9 illustrates results of the tri-frequency reactor using various combinations of frequencies and H_2O_2 concentrations. The combination that archived the highest destruction amount was all three frequencies with 51 µM H_2O_2/sec addition. The difference in the disinfection with and without H_2O_2 was small. The control illustrated that the sample was being completely mixed throughout the system. The 1.7-mHz frequency by itself had a minimal affect on the *Cryptosporidium* concentration.

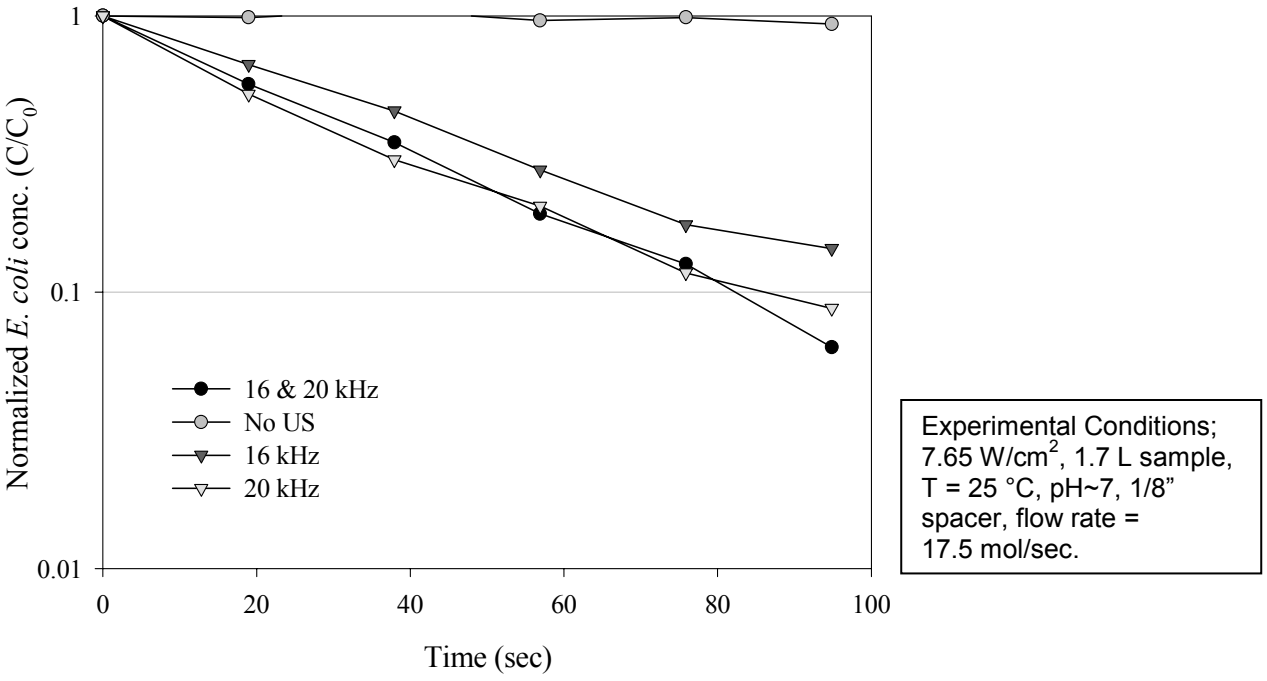

Figure 3-6 – Effect of Ultrasonic Frequency on *E. coli* Disinfection.

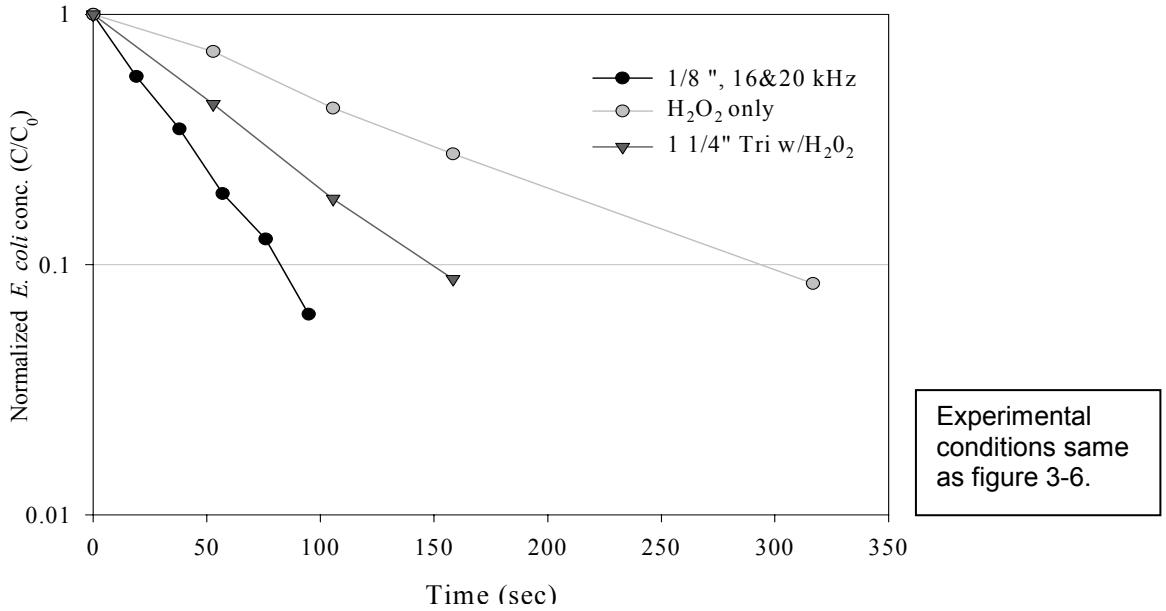

Figure 3-7– Effect of Spacer Width, Frequency and H_2O_2 Addition on *E. coli* Disinfection.

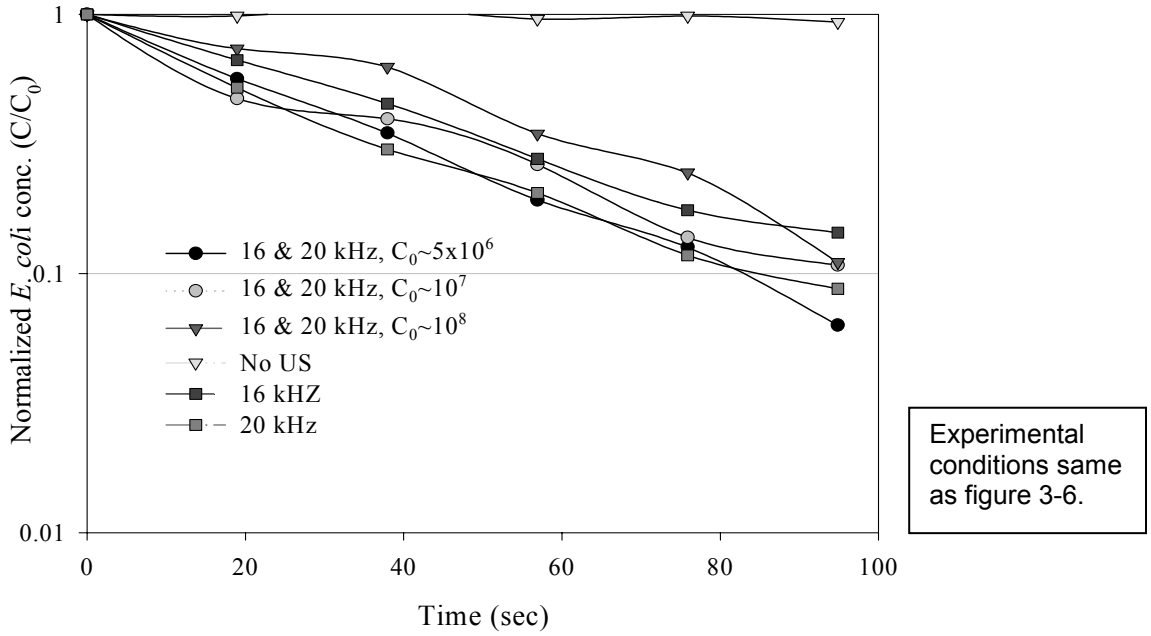

Figure 3-8 – Effect of Frequency and Frequency Combinations on *E. coli* Disinfection.

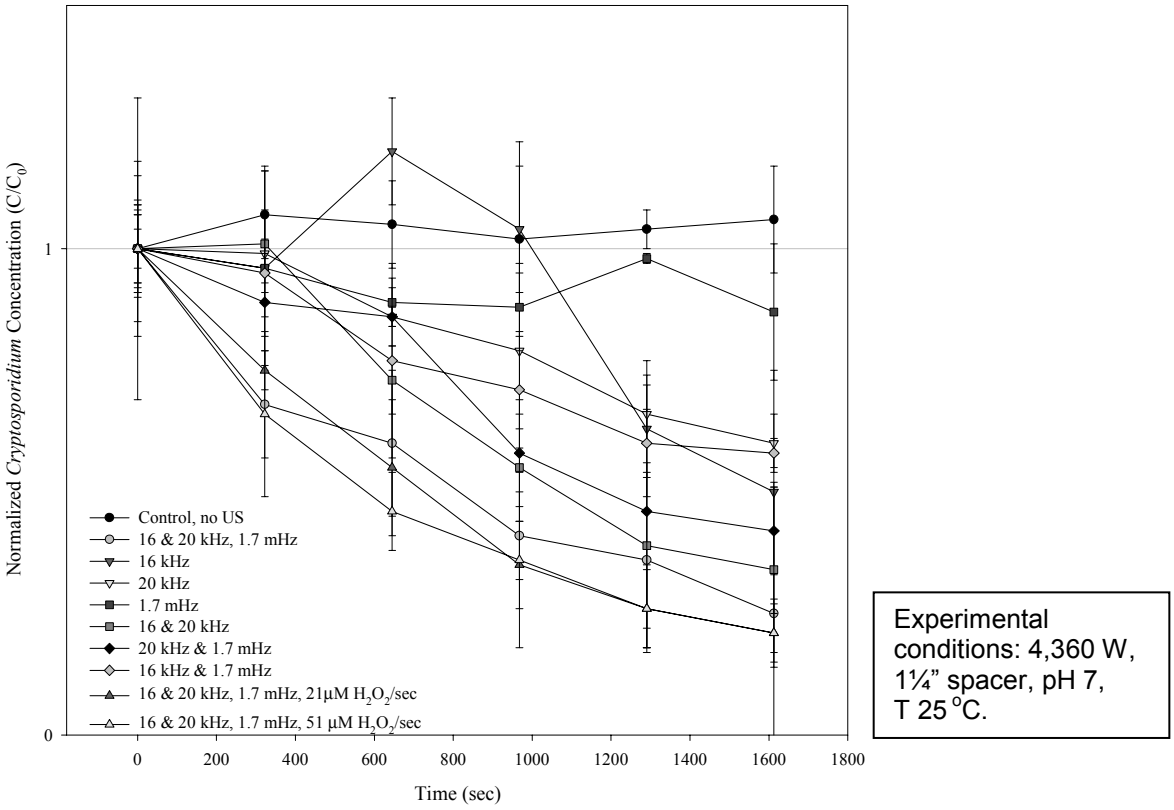

Figure 3-9 – *Cryptosporidium* Destruction, Tri-frequency Reactor.

Figure 3-10 illustrates the H_2O_2 concentration in the system versus the destruction of the Cryptosporidium. A 0.3 percent solution of H_2O_2 was continuously pumped into the reaction chamber at different speeds. After 1600 seconds of reaction time, a total of 90 mL of the solution was introduced into the system when the pump was set on speed level 2 (21 µM H_2O_2/sec), 190 mL at speed level 3 (51 µM H_2O_2/sec). The H_2O_2 concentration was measured using a HP Spectrophotometer. It appears that the maximum concentration in the reactor is 12 mM.

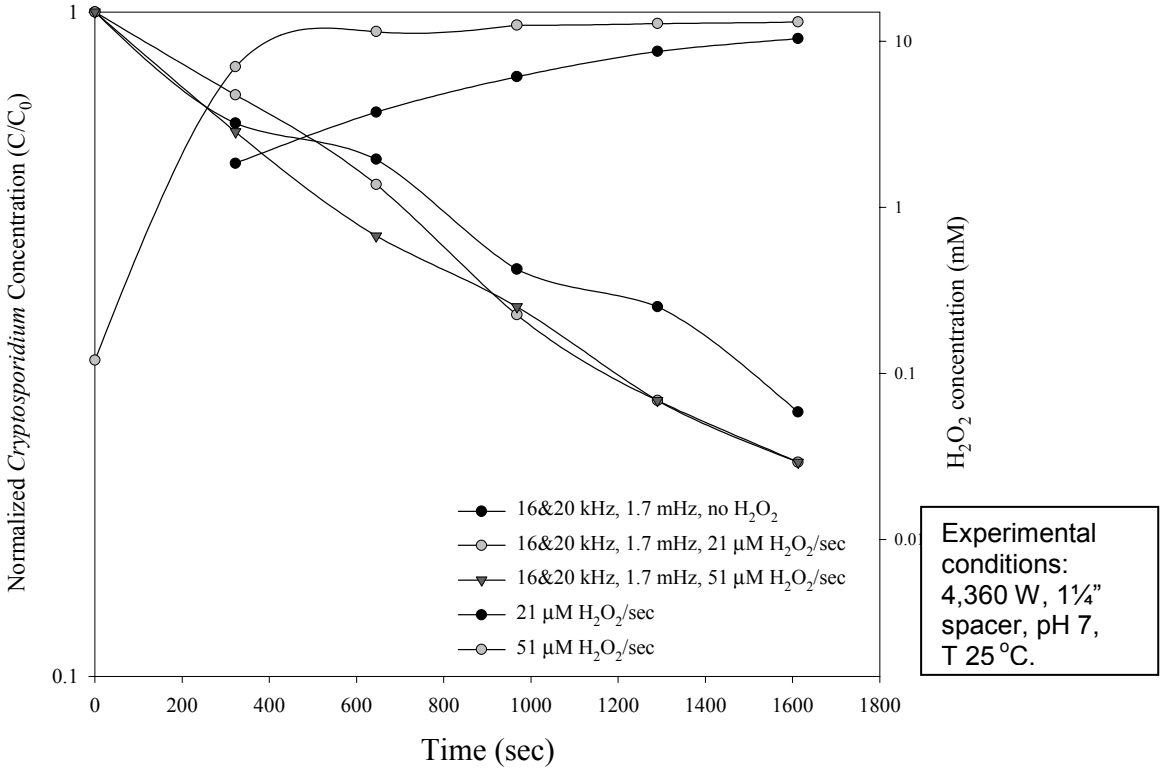

Figure 3-10 – *Cryptosporidium* Destruction Versus H_2O_2 Concentration, Tri-frequency Reactor.

Figure 3-11 illustrates the effect of individual frequencies on the disinfection of Cryptosporidium parvum. The tri-frequency spacer was used with only one transducer set turned on. The most effective frequency is 16 kHz, followed by 20 kHz and finally 1.7 mHz. The 1.7 mHz was substantially less effective than the lower frequencies, giving some support to the hypothesis that the destruction of Cryptosporidium is primarily a physical process. However, no absolute conclusion can be made because the 1.7-mHz waves are traveling parallel to the 16 and 20 kHz transducer plates, making the distance that they travel 3" instead of 1¼". In addition, the total power output of the 1.7-mHz transducers is only 360 W compared to the 16- or 20-kHz transducers that provide 2,000 W each.

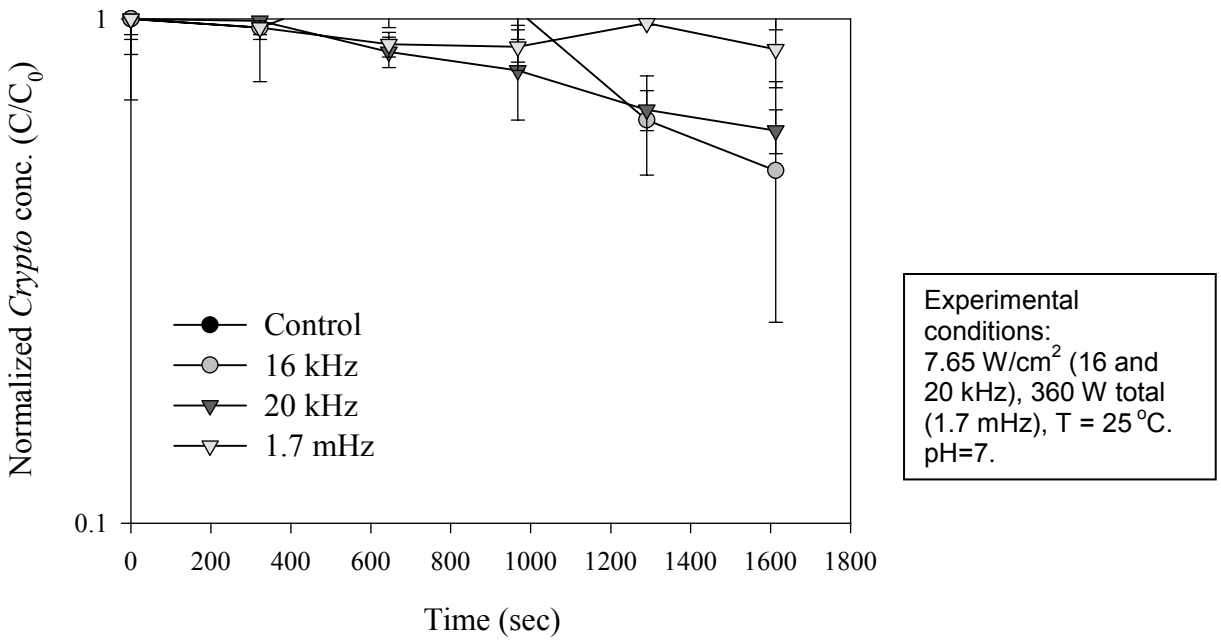

Figure 3-11 – Effect of a Single Frequency on *Cryptosporidium* Disinfection Using the 1¼" Tri-frequency Spacer.

Figure 3-12 illustrates the disinfection of *Cryptosporidium* when a combination of frequencies are used. The waves are additive so the relative pressure amplitude is increased because of the effect of superposition. The single low frequency (16 or 20 kHz) combined with the high frequency (1.7 mHz) performed better than the individual low frequency alone but did not perform as well as when the two low frequencies were combined. The combination of all three frequencies provided the most destruction, followed by the 16- and 20-kHz combination.

Although physical destruction is the most probable mechanism of oocyst destruction, the effect of the addition H_2O_2 to increase the OH• was investigated. Figure 3-13 illustrates the best combination of frequencies (16 and 20 kHz, 1.7 mHz) with different dosages of H_2O_2 continuously fed into the reaction chamber. The tri-frequency combination with the highest dosage of H_2O_2 provided the largest decrease in oocyst concentration but the effect was not dramatic, again reinforcing the hypothesis that the majority of oocysts are in fact being shattered by the physical processes (high pressure and temperature).

3.3 Conclusions

The qualification and quantification system utilizing the dual-lamp/dual filter system improved upon EPA Method 1623 and provided the ability to view FITC and DAPI labeled samples simultaneously. The examination time was reduced by at least 50 percent and the issue of spatial positioning of the oocysts relative to the sporozoites was resolved.

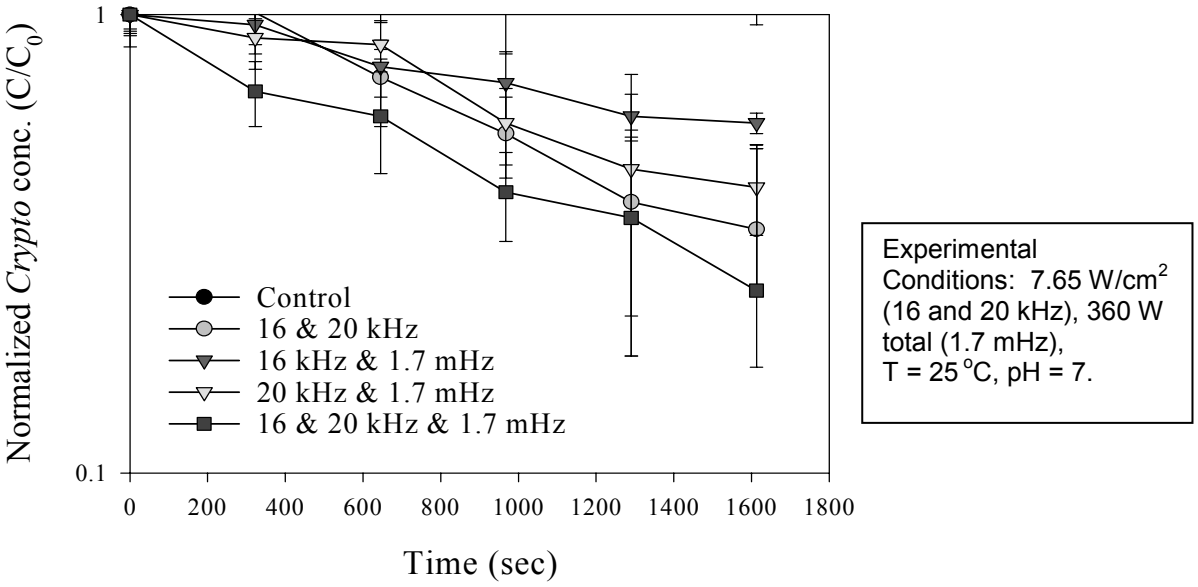

Figure 3-12 – Effect of a Combination of Frequencies on *Cryptosporidium* Disinfection using the 1 ¼" Tri-frequency Spacer.

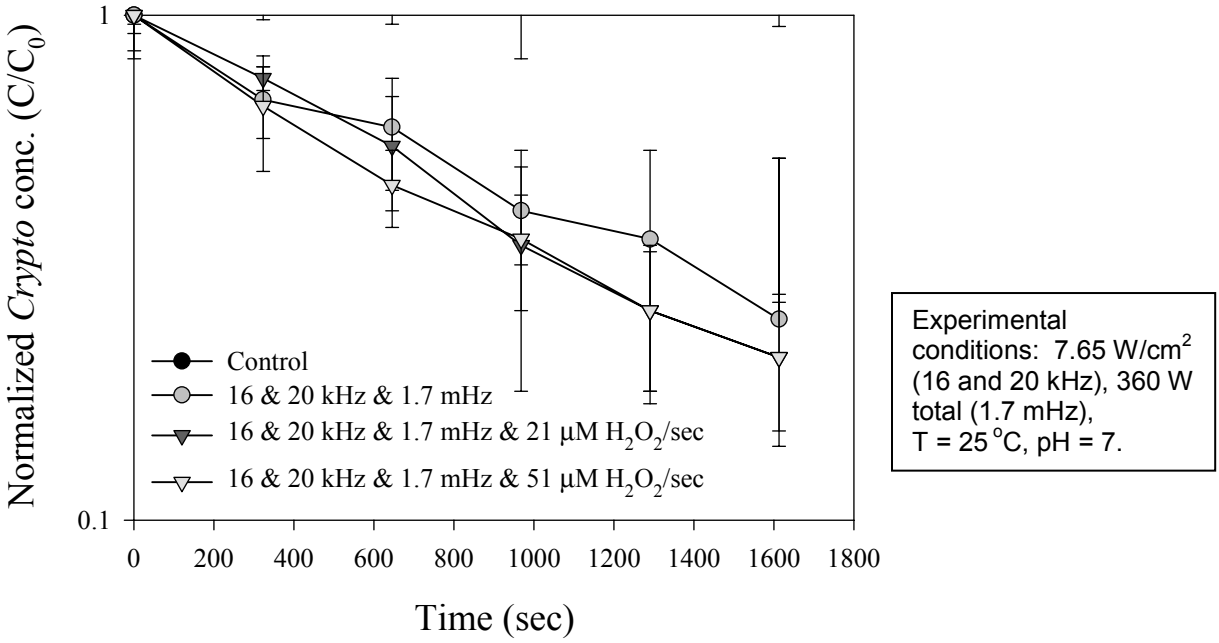

Figure 3-13 – Effect of a Combination of Frequencies with H_2O_2 on *Cryptosporidium* Disinfection Using the 1 ¼" Tri-frequency Spacer.

The final version of the Nearfield™ Acoustical Processor with the tri-frequency spacer proved to function satisfactorily from a physical and engineering standpoint but did not increase the destruction capabilities of the system with respect to *Cryptosporidium* as much as hoped. It is hypothesized that the primary mechanism of oocyst destruction is physical. It did help with respect to *E. coli* disinfection, a process that is more heavily impacted by the oxidation capabilities of the OH•. After discovering that the time scale of THMFP reduction and *Cryptosporidium* destruction was very different, it was suspected that this process would be limited by its financial feasibility with respect to organic mineralization. Future work with the H_2O_2 and tri-frequency combination may prove this assumption to be incorrect.

It has been clearly demonstrated that the ultrasonic process is capable of disinfection and organic mineralization. Both the ultrasonic system and the imaging and identification systems have been built so the tools are available for future researchers to optimize the process and develop it into a financially feasible one.

4. References

Beardsley, T., 1993, Putting a spin on parasites. *Sci. Am*., 269: 103.

Chapman, P.A., Rush, B.A., McLauchlin, J., (1990), An enzyme immunoassay for detecting *Cryptosporidium* in fecal and environmental samples. *J. Med. Microbiol*., 32: 233-237.

Entezari, M.H., Kruus, P., 1996, Effect of frequency on sonochemical reactions II. Temperature and intensity effects. *Ultrasonic. Sonochem*. 3: 19-24.

EPA Method 1623: *Cryptosporidium* and *Giardia* in Water by Filtration/IMS/FA, 1999. http://www.epa.gov/ost/methods/1623.pdf, EPA-821-R-99-006.

Hua, I., Hoffmann, M.R., 1997, Optimization of ultrasonic irradiation as an advanced oxidation technology. *Environ. Sci. Technol*., 31: 2237-2243.

Huang, C.P., Myoda, S.P., Chiu, P., Kim, I.K., Sung. M., 2000, Treatment of waste waters for water reuses by a catalytic sonochemical process. Final Technical Report, Bureau of Recalamation – Department of the Interior.

Johnson, D.W., Pieniazek, N.J., Griffin, D.W., Misener, L., Rose, J.B., 1995 Development of a PCR protocol for sensitive detection of *Cryptosporidium* oocysts in water samples. *Applied and Environmental Microbiology*, 611(11): 3849-3855.

Upton, S.J., Tilley, M., Nesterenko, M.V., Brillhart, D.B., 1994, A simple and reliable method of producing *in vitro* infections of *Cryptosporidium parvum* (Apicomplexa). *FEMS Microbiol*., 118: 45-49.

Vesey, G., Slade, J.S., Byrne, M., Shepherd, K., Dennis, P.J., Fricker, C.R., 1993, Routine monitoring of *Cryptosporidium* oocysts in water using flow cytometry. *J. Appl. Bacteriol*., 75: 87-90.

Webster, K.A., Pow, J.D.E., Giles, N., Catchpole, J., Woodward, M.J., 1993, Detection of *Cryptosporidium* parvum using a specific polymerase chain reaction. *Vet. Parasitol.*, 50(1-2): 35-44.

Wehner, J.F. and R.H. Wilhelm, 1956, Boundary conditions of flow reactor. *Chemical Engineering Science*, 6: 89-93.

Appendix A:

Statistical Analysis of Selective Figures

Figure 6-6, Paired t-test

16 kHz and 20 kHz and No US
T value -4.3733032162
P value0.0071997005
Degrees of Freedom 5

16 kHz and 20 kHz and 16 kHz
T value -4.3319250285
P value0.0074857417
Degrees of Freedom 5

16 kHz and 20 kHz and 20 kHz
T value 0.8762507798
P value0.4209901275
Degrees of Freedom 5

No US and 16 kHz
T value 4.1324937903
P value0.0090629575
Degrees of Freedom 5

No US and 20 kHz
T value 4.5101296419
P value0.0063401434
Degrees of Freedom 5

16 kHz and 20 kHz
T value 3.3981558714
P value0.0192896249
Degrees of Freedom 5

Figure 6-8, Paired t-test

16 and 20 kHz ($5x10^6$) and 16 and 20 kHz (10^7)
T value -0.5805230270
P value0.5867417049
Degrees of Freedom 5

16 and 20 kHz ($5x10^6$) and 16 and 20 kHz (10^8)
T value -3.2001534780
P value0.0239910622
Degrees of Freedom 5

16 and 20 kHz ($5x10^6$) and No US
T value -4.3733032162
P value0.0071997005
Degrees of Freedom 5

16 and 20 kHz ($5x10^6$) and 16 kHz
T value -4.3319250285
P value0.0074857417
Degrees of Freedom 5

16 and 20 kHz ($5x10^6$) and 20 kHz
T value 0.8762507798
P value0.4209901275
Degrees of Freedom 5

16 and 20 kHz (10^7) and 16 and 20 kHz (10^8)
T value -2.5071372902
P value0.0540166374
Degrees of Freedom 5

16 and 20 kHz (10^7) and No US
T value -4.6034763467
P value0.0058219283
Degrees of Freedom 5

16 and 20 kHz (10^7) and 16 kHz
T value -1.9706838560
P value0.1058313988
Degrees of Freedom 5

16 and 20 kHz (10^7) and 20 kHz
T value 1.2164485396
P value0.2781001512
Degrees of Freedom 5

16 and 20 kHz (10^8) and No US
T value -3.7086716320
P value0.0138740025
Degrees of Freedom 5

16 and 20 kHz (10^8) and 16 kHz
T value 1.9946339987
P value0.1026405329
Degrees of Freedom 5

16 and 20 kHz (10^8) and 20 kHz
T value 2.8034829562
P value0.0378378341
Degrees of Freedom 5

No Us and 16 kHz
T value 4.1324937903
P value0.0090629575
Degrees of Freedom 5

No US and 20 kHz
T value 4.5101296419
P value0.0063401434
Degrees of Freedom 5

16 kHz and 20 kHz
T value 3.3981558714
P value0.0192896249
Degrees of Freedom 5

Figure 6-11, Paired t-test

Control and 16 kHz
T value 1.3499344285
P value0.2349283880
Degrees of Freedom 5

Control and 20 kHz
T value 3.1361872496
P value0.0257769038
Degrees of Freedom 5

Control and 1.7 mHz
T value 3.8570778033
P value0.0119152493
Degrees of Freedom 5

16 kHz and 20 kHz
T value 0.9841595053
P value0.3702323583
Degrees of Freedom 5

16 kHz and 1.7 mHz
T value -0.3748416628
P value0.7231514423
Degrees of Freedom 5

20 kHz and 1.7 mHz
T value -1.8877239866
P value0.1177034608
Degrees of Freedom 5

Figure 6-12, Paired t-test
Control and 16 and 20 kHz
T value 3.0331944905
P value0.0289753396
Degrees of Freedom 5

Control and 16 kHz and 1.7 mHz
T value 3.6079964541
P value0.0154128903
Degrees of Freedom 5

Control and 20 kHz and 1.7 mHz
T value 3.2693492470
P value0.0222145485
Degrees of Freedom 5

Control and 16 and 20 kHz and 1.7 mHz
T value 4.2193326683
P value0.0083331448
Degrees of Freedom 5

16 and 20 kHz and 16 kHz and 1.7 mHz
T value -1.9734759423
P value0.1054541484
Degrees of Freedom 5

16 and 20 kHz and 20 kHz and 1.7 mHz
T value -0.8958676933
P value0.4113746173
Degrees of Freedom 5

16 and 20 kHz and 16 and 20 kHz and 1.7 mHz
T value 2.5205041513
P value0.0531419535
Degrees of Freedom 5

16 kHz and 1.7 mHz and 20 kHz and 1.7 mHz
T value 1.6819198298
P value0.1534112697
Degrees of Freedom 5

16 kHz and 1.7 mHz and 16 and 20 kHz and 1.7 mHz
T value 4.4479673098
P value0.0067149877
Degrees of Freedom 5

20 kHz and 1.7 mHz and 16 and 20 kHz and 1.7 mHz
T value 4.0786265896
P value0.0095527173
Degrees of Freedom 5

Figure 6-13, Paired t-test
Control and 16 and 20 kHz and 1.7 mHz
T value 4.2193326683
P value0.0083331448
Degrees of Freedom 5

Control and 16 and 20 kHz and 1.7 mHz and 21 µM H_2O_2/sec
T value 3.9890001756
P value0.0104368475
Degrees of Freedom 5

Control and 16 and 20 kHz and1.7 mHz and 51 µM H_2O_2/sec
T value 4.3409133976
P value0.0074225038
Degrees of Freedom 5

16 and 20 kHz and1.7 mHz and 16 and 20 kHz and 1.7 mHz and 21 µM H_2O_2/sec
T value 1.2529036044
P value0.2656428424
Degrees of Freedom 5

16 and 20 kHz and 1.7 mHz and 16 and 20 kHz & 1.7 mHz & 51 µM H_2O_2/sec
T value 2.7313758674
P value0.0412127215
Degrees of Freedom 5

16 and 20 kHz and 1.7 mHz and 21 µM H_2O_2/sec and 16 and 20 kHz and 1.7 mHz and 51 µM H_2O_2/sec
T value 1.4481858929
P value0.2072292660
Degrees of Freedom 5

Appendix B: HyperTerminal Interface for Prior Automated Stage

The Prior Stage can be controlled automatically using an RS-232 computer interface and HyperTerminal. To set up the HyperTerminal follow these instructions:

Click on the Start button, click on Run and type "hypertrm.exe", and click OK. After the Connection description dialog box appears type in "Stage" and click OK.

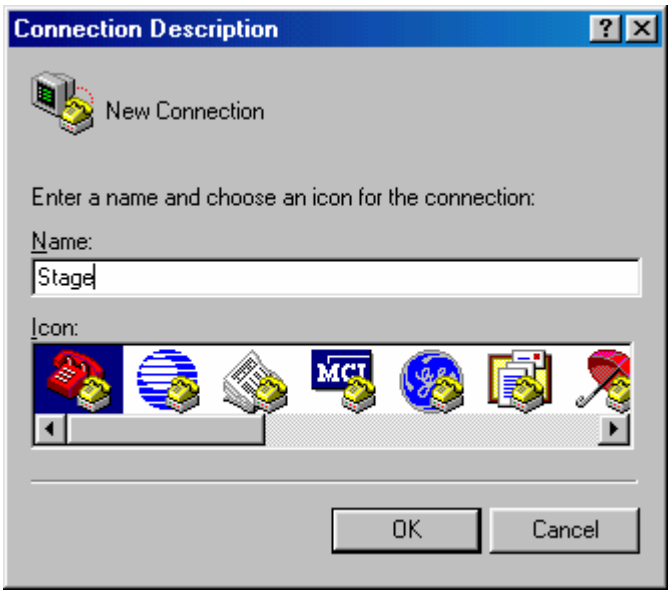

You must now select the communication port to which your controller is connected. Under "Connect using"" select the proper port (either 1, 2, 3, or 4) then click OK.

Once you select the COM port you must enter the following settings:

1. Bits per second 9600
2. Data bits 8
3. Parity None
4. Stop bits 1
5. Flow control None

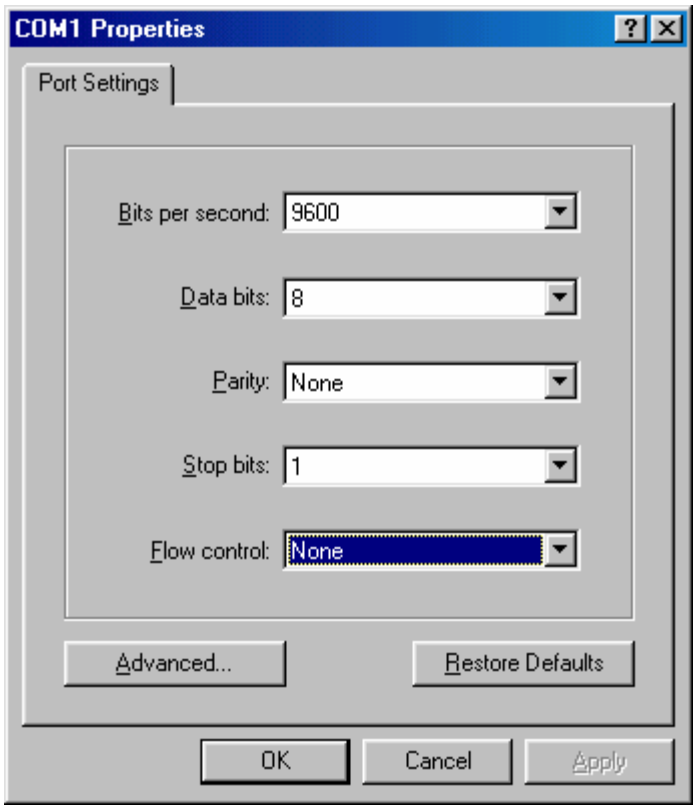

After you click OK, you will have a blank screen. Go to the top left of the window and click on File then Properties. Click on the "Settings" tab and select ASC11 Setup.

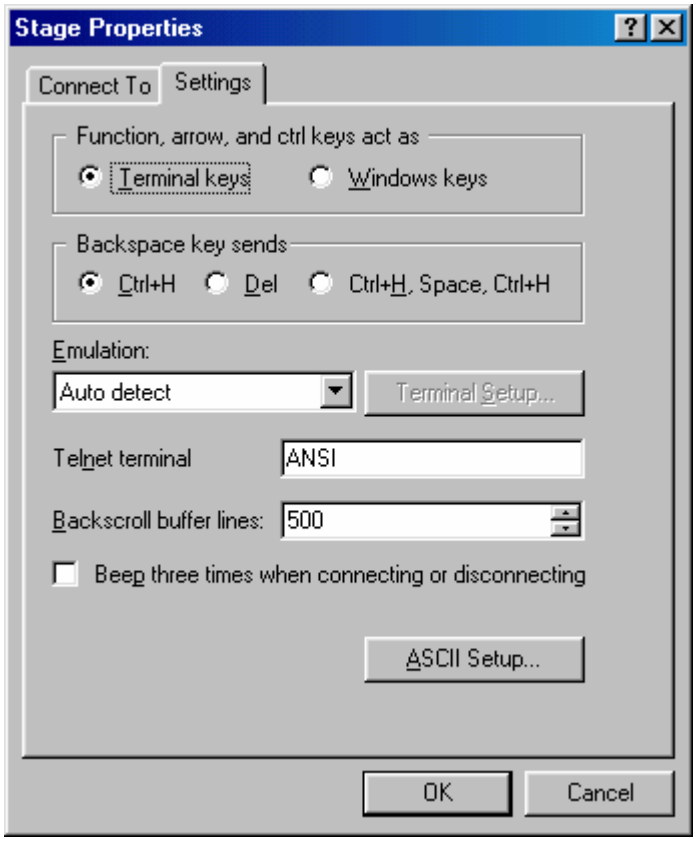

Once you are in the ASC11 Setup screen select:

1. Echo typed characters locally (under ASC11 Sending)

2. Append Line feeds to incoming line ends (ASC11 Receiving)

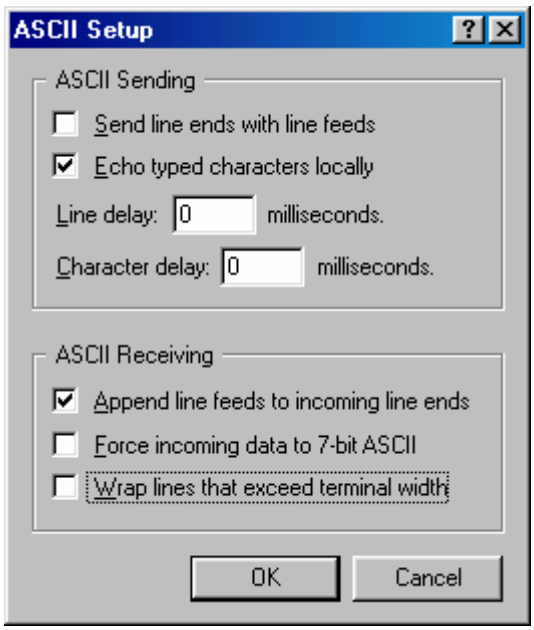

Click OK and OK. Hit the Enter key and you should see the position, i.e., 7648, 26523, 1345. The following are a list of the commands that can be sent to the control box from the host computer. The system will accept upper or lower case letters.

The column, "PC Send", details the command letter; data to set variables, and the 0D Hex (0D Hex is the keyboard "Enter" key) the control code is shown as [0D]. All commands are sent as an ASCII string with no spaces between the characters. Where variables are set, the data is separated by commas (2C Hex). Where no data is required, the command letter followed by [0D] is all that is necessary.

The second column, "Reply," is the ASCII string that will be returned to the host computer when the operation has been completed. In the case of commands that set variables, the command will be sent in less than 10 microseconds. In the case of those which initiate movement, the reply will be sent upon completion of the operation. Software control of H128/H101 should ensure that the returned characters are recognized before new commands are sent.

The third column, "Operation," specifies what action will occur or the purpose of the variables being defined. It also gives the limit that the control box will accept.

PC Send	Reply	Operation
Z[0D]	0[0D]	X, Y, and Z absolute positions are set to zero. Used for initializing the stage at any position within the envelope of its travel. All variables set by these commands are retained in battery backed memory by the processor.
X, n, m	0[0D]	Where “n” and “m” are the number of pulses to be moved between fields in the X and Y axes of a raster or snake pattern.
N, n, m[0D]	0[0D]	Where “n”” and “m” are the number of fields in X and Y respectively, used to set up the raster and snake pattern. The number of fields to be viewed in the axis is 1 more than the data input, e.g., N, 0, 5[0D] would set a raster with a straight line in the Y axis consisting of 6 positions. The “X” commands sets the distance between fields.
S[0D]	R[0D]	Move to the next field in the raster pattern. At the end of the pattern the stage will return to the raster origin.
L[0D]	R[0D]	Move left the number of pulses as defined in the “x” command (variable “n”).
R[0D]	R[0D]	Same as L[0D] but move to the right.
F[0D]	R[0D]	Move to the front the number of pulses as defined in the “X” command (variable “m”).
B[0D]	R[0D]	Same as F[0D] but move to the back
G, x, y[0D]	R[0D]	Move to the “x” (X axis) and “y” (Y axis) absolute positions. The permitted values of “x” and “y” must be between ± 7,000,000.
G3, x, y, z[0D]	R[0D]	Move to the “x” (X axis), “y” (Y axis), and “z” (Z axis) absolute positions. The X axis and Y axis movements are done simultaneously and once completed, the Z axis movement is implemented.

Appendix C:
X-keys™ Keyboard Programming

The X-keys™ keyboard allows the HyperTerminal command strings that control the stage to be input by a single keystroke. After installing the keyboard (use the "Y" adapter to plug in both the primary keyboard and the X-keys™ into the PS/2 keyboard computer input), program the keys using the following procedure:

1. Slide the program switch to the UP program position (a red indicator will be visible to the left of the switch). Note: The num lock, caps lock, and scroll lock lights will sequentially blink.

2. Tap the key on the X-keys™ that you want to program. Note: The num lock, caps lock, and scroll lock lights will stop blinking and stay on.

3. Type (on the main keyboard) the key sequence to be programmed into the key on the X-keys™.

4. When the sequence is complete, tap the key on the X-keys™ again.

5. Repeat steps 2, 3, and 4 to program additional keys.

6. When programming is complete, slide the program switch DOWN to the run position.

Appendix D: Dual Lamp Scope Housing

This appendix is to be used as a supplement to the Olympus Provis AX instruction manual. A second halogen lamp housing has been added to the Olympus AX70 microscope using a modified 20/20 Technology DS_90 lamp housing. Emission filters (A: DAPI – narrow UV top position, wide UV bottom position, B: FITC w/KGB glass – top position, bottom position empty) have been installed on the filter sliders between the lamp housing and DS_90. The line on the control knob indicates the position of the dichroic mirror (FITC pass through, DAPI reflects) within the DS_90 housing. Parallel to the connection tube allows only B light (FITC emission) through while a position normal to the connection tube allows both lamp A & B light (FITC & DAPI emission) to reach the microscope.

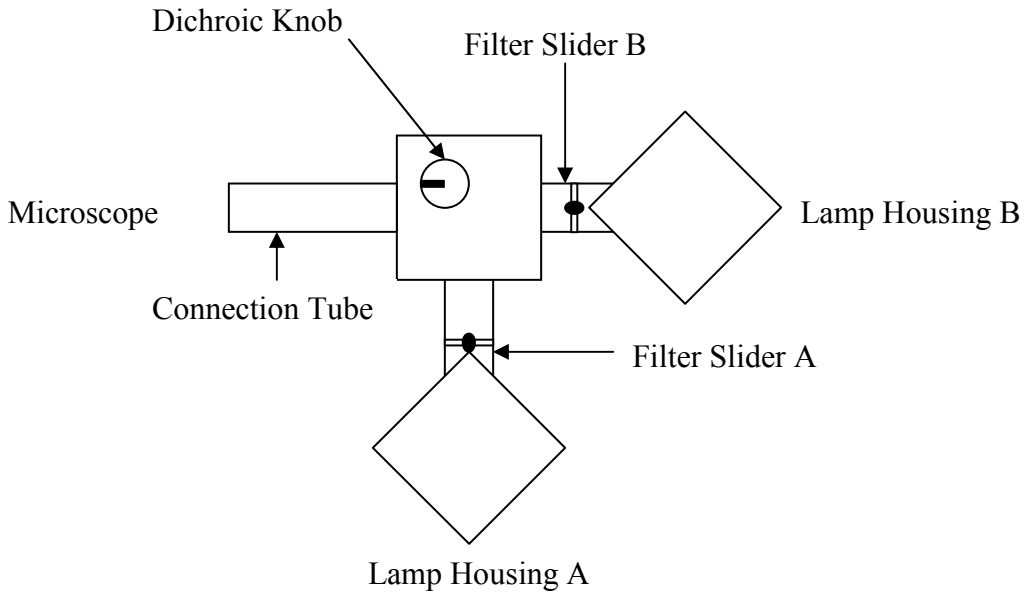

Figure D-1 – Dual Lamp Housing.

Appendix E:
AutoCAD Reactor Drawings

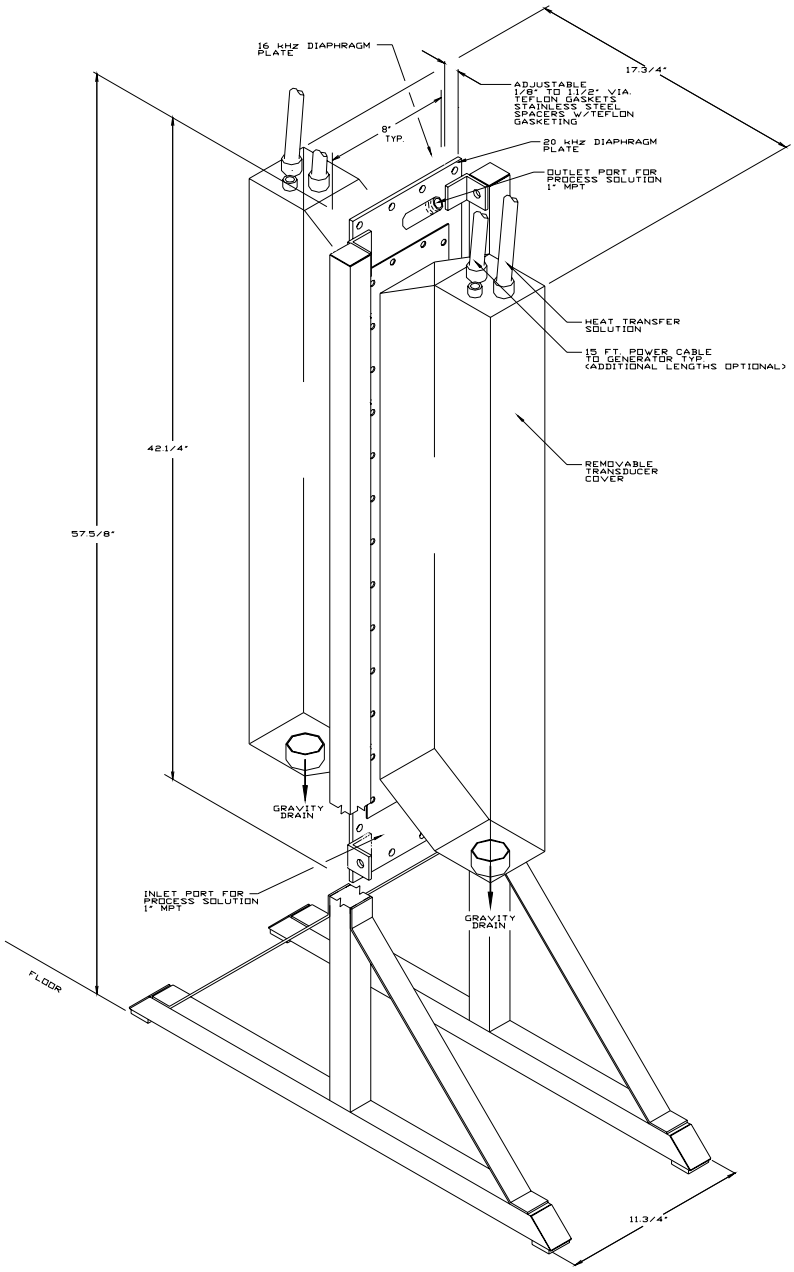

Figure E-1 – Nearfield™ Reactor Schematic.

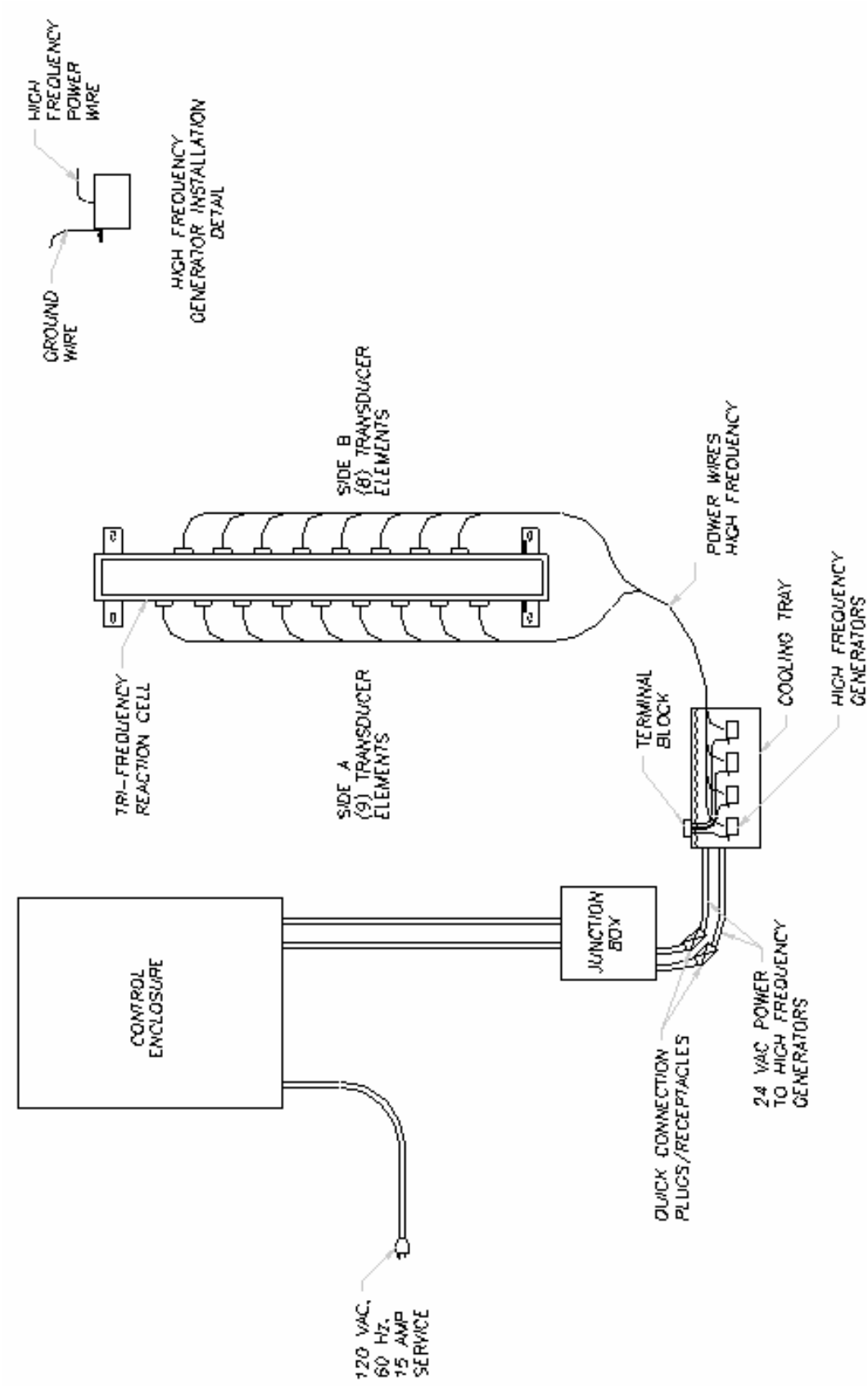

Figure E-2 – Tri-frequency Spacer Wiring Schematic.

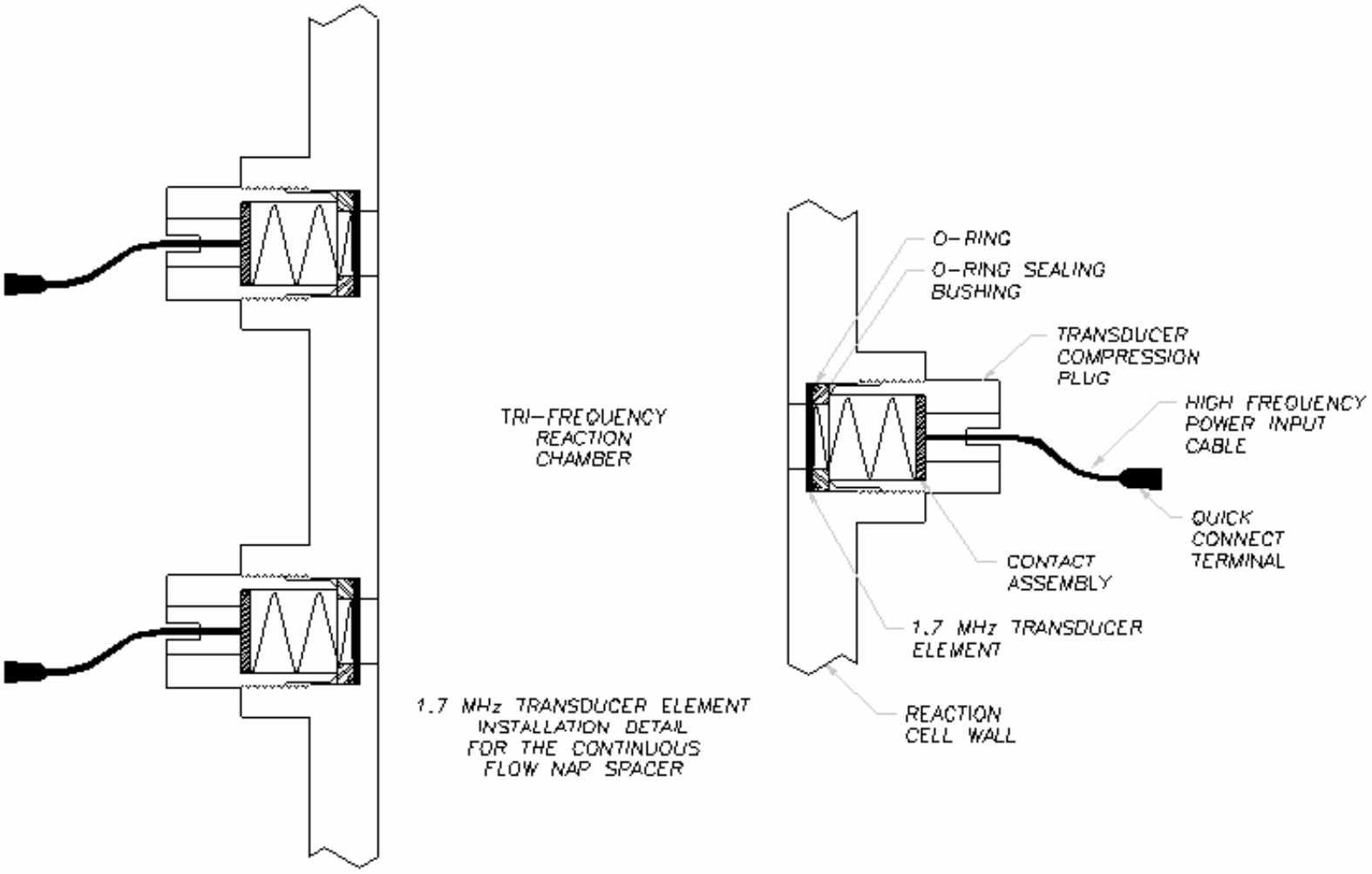

Figure E-3 – Tri-frequency 1.7-mHz Transducers Embedded in Spacer Wall.

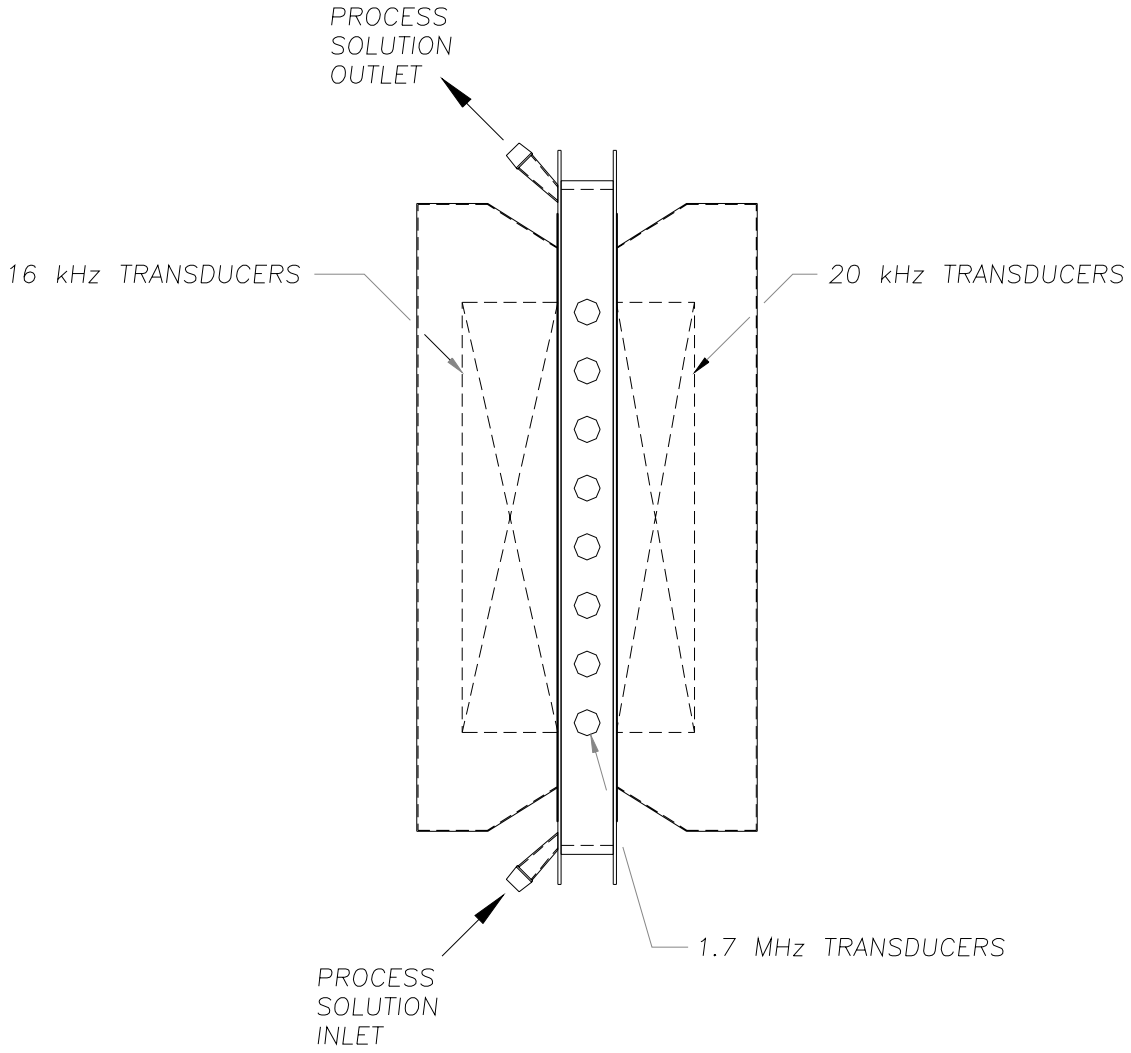

Figure E-4 – Overview of Tri-frequency Placement within Nearfield™ Reactor.